Marine Geophysical Research (2019) 40:395–418
https://doi.org/10.1007/s11001-019-09379-5

ORIGINAL RESEARCH PAPER

Crustal structure of an extinct, late Jurassic-to-earliest Cretaceous spreading center and its adjacent oceanic crust in the eastern Gulf of Mexico

Pin Lin[1,3] · **Dale E. Bird**[1,2] · **Paul Mann**[1]

Received: 11 August 2018 / Accepted: 21 January 2019 / Published online: 9 February 2019

Abstract
An extinct, late Jurassic-to-earliest Cretaceous ridge-and-fracture zone geometry in the western Gulf of Mexico (GOM), and extinct seafloor ridge segments in the eastern Gulf of Mexico (EGOM), were previously identified using the vertical gradient of satellite-derived free-air gravity data. Circular gravity anomaly lows, and magnetic anomaly highs, over the center of spreading ridge segments are interpreted as large volcanic centers that erupted within a late Jurassic-to-earliest Cretaceous, slow-spreading center. Detailed mapping of oceanic basement using oil industry seismic data indicates that the EGOM oceanic ridge system is characterized by 30-60-km-long spreading ridge segments, that include 15-km-wide, 2-km-high axial volcanoes in their centers, and nodal basins at their ends. Stratigraphic evidence from seismic reflection data tied to a deepwater well indicates that volcanism along the spreading ridge ended around the same time (Berriasian), or slightly after (Valanginian), the cessation of seafloor spreading in the EGOM. Flowlines of late Jurassic-to-earliest Cretaceous seafloor, based on a pole of rotation from the geometry of GOM spreading ridges and fracture zones, show a good match with gravity and magnetic anomalies along the Florida and Yucatan conjugate margins of the EGOM. Mapping of age-dated, stratigraphic downlaps onto the oceanic crust is consistent with an interpreted ridge jump at the beginning of seafloor spreading (Kimmeridgian) to the southwest, and in the same southwestward direction of a previously inferred mantle plume in the central GOM. Our 3-D gravity structural inversion of the Moho requires 6.4 km thick oceanic crust in the northwestern EGOM, and 5.5 km thick oceanic crust in southeastern EGOM. We interpret this along-ridge, thickness variation to reflect faster spreading and thicker oceanic crust farther from the opening pole located in the southeastern GOM.

Keywords Eastern Gulf of Mexico · Extinct spreading ridge · Post-spreading magmatism · Oceanic crustal structure · 3-D gravity modeling

Introduction and significance

Sandwell et al. (2014) used satellite-derived gravity data to interpret: (1) a 490-km-long, relict, system of short oceanic spreading ridges separated by long fracture zones in the western GOM; and (2) a 286-km-long, system of short spreading ridge segments in eastern GOM (EGOM) that are separated by short, but recognizable, right-lateral, northeast-southwest-trending offsets (Fig. 1a, b). Deep-penetration, 2D and 3D seismic reflection surveys by the oil industry in the deepwater GOM have imaged several aspects of the structure and post-spreading stratigraphy of the extinct, spreading system (Stephens 2001; Imbert and Philippe 2005; Snedden et al. 2013, 2014; Kegel et al. 2016).

Stephens (2001) identified basement highs in the vicinity of the ridge segments as "buried hills" along with intervening basins based on 2D seismic data in the northwestern part of the EGOM (Fig. 1a). Stephens (2001) also suggested that large, buried hills are seamounts that formed within transform fault valleys, leading him to further suggest a Jurassic pattern of northeast-trending spreading ridges offset by northwest-trending transform faults. Using the same 2D seismic dataset, Imbert (2005a, b), and Imbert

✉ Pin Lin
slyzlinpin@163.com

[1] Department of Earth and Atmospheric Sciences, University of Houston, Houston, Texas 77204-5007, USA

[2] Bird Geophysical, Houston, TX 77084, USA

[3] Research Institute, CNOOC China Ltd-Beijing, Beijing 100001, China

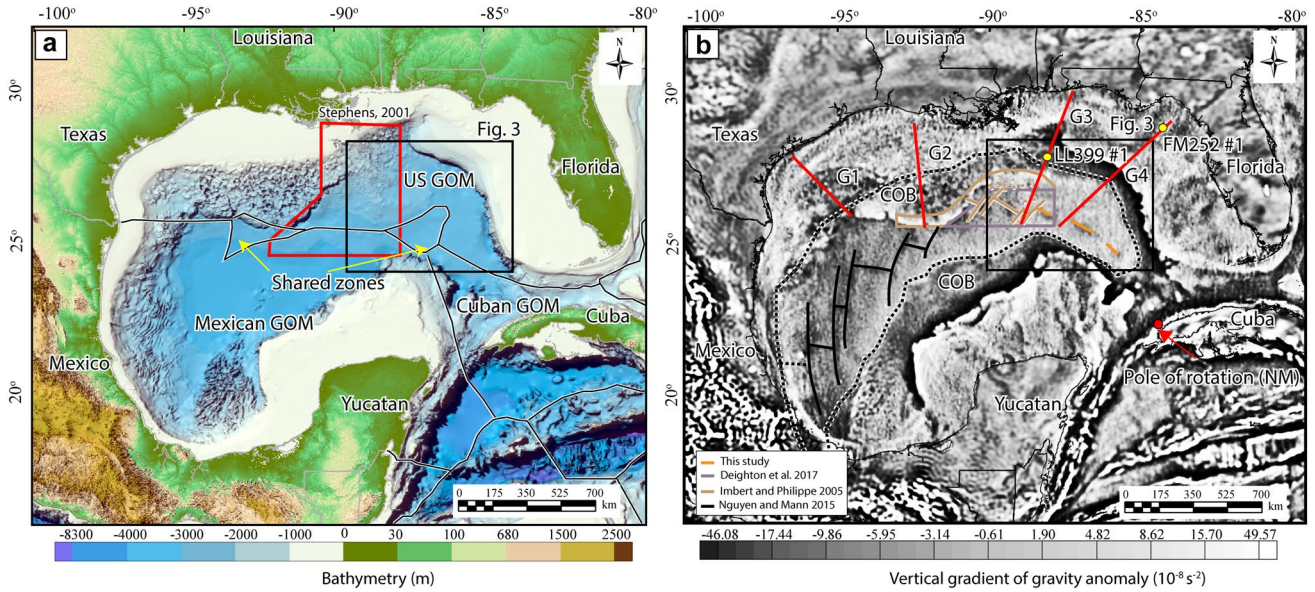

Fig. 1 **a** Geographic setting of the Gulf of Mexico basin (GOM) with bathymetry taken from the GEBCO bathymetric compilation by Jakobsson et al. (2012). Red box shows the study area of Stephens (2001). Black boxed area shows the eastern Gulf of Mexico (EGOM) study area described in this paper. **b** Vertical gradient of free-air gravity (VGG) anomalies of the GOM showing the slightly darker, linear expression of the extinct and deeply buried, spreading ridge-and-fracture zone system of late Jurassic-to-earliest age (Sandwell et al. 2014). Solid black and yellow lines represent ridge segments and fracture zones identified from Nguyen and Mann (2016) and this study, respectively; less pronounced ridges and fracture zones are shown as dotted lines. The solid brown lines represent spreading ridges, fracture zones, pseudo-faults, and the study area of Imbert and Philippe (2005). Purple lines show the study area of Deighton et al. (2017). Red lines show the locations of refraction profiles from the Gulf of Mexico Opening (GUMBO) project (Christeson et al. 2014; Eddy et al. 2014). The red dot indicates the location of the late Jurassic-to-earliest Cretaceous pole of rotation for the GOM. The location of this pole was determined from the curvilinear pattern of fracture zones across the entire GOM (Nguyen and Mann 2016)

and Philippe (2005) incorporated high resolution, magnetic data to propose a spreading direction orthogonal to that of Stephens (2001), with northwest-oriented spreading ridges offset by northeast-trending transforms (Fig. 1b). Several studies have noted close alignment between seamounts and positive magnetic anomalies, suggesting the presence of an oceanic spreading center that is now buried beneath 6–8 km of Mesozoic–Cenozoic sedimentary rocks in the deep-water GOM (Hall and Najmuddin 1994; Imbert and Philippe 2005; Nguyen and Mann 2016).

Snedden et al. (2014) interpreted industry 2D seismic data that includes the extinct spreading ridge but including a larger region of the EGOM. These authors mapped discontinuous valleys within the basement that they interpreted to be discrete sections of a northwest-trending Jurassic spreading system. Snedden et al. (2014) also proposed that basement highs along the spreading axis were seamounts that formed along the axial spreading ridge and that were probably related to local variations in magma supply, as commonly observed along active slow-spreading ridges worldwide (Macdonald and Fox 1993) (Fig. 3). Deighton et al. (2017) mapped a long fracture zone in the western GOM using 3D seismic data. The curved fracture zone is characterized by an 8–10-km-wide trough filled with 200–400 ms (300–600 m) of sediments.

Another important feature related to EGOM seafloor spreading is the continent-ocean boundary (COB) along the conjugate margins of Florida and Yucatan. The exact location of COB in the GOM has been a topic of much debate over the years with sparse refraction, reflection controls and lack of recognizable magnetic anomalies (Sawyer et al. 1991; Marton and Buffler 1994; Bird et al. 2005; Pindell and Kennan 2009; Hudec et al. 2013; Christeson et al. 2014; Eddy et al. 2014). Nguyen and Mann (2016) not only mapped the remotely-imaged pattern of oceanic spreading ridge-and-fracture zone geometries, but were also able to define the location of the continent-ocean boundary (COB) in the southern GOM using the tilt derivative of residual Bouguer gravity anomalies and vertical gravity gradient data from Sandwell et al. (2014). Nguyen and Mann (2016) proposed a 37° counterclockwise rotation of the Yucatan block about a single pole of rotation located near northwestern Cuba from the curvature of GOM fracture zones and spreading ridges, especially in the western GOM (Fig. 1b). Prior to the availability of the Sandwell et al. (2014) high-resolution marine-satellite gravity data,

several studies proposed that the Yucatan block had undergone a Mesozoic counterclockwise rotation through angles ranging from 40° to 60° (Hall and Najmuddin 1994; Marton and Buffler 1994; Bird et al. 2005; Pindell and Kennan 2009). This rotation of the Yucatan continental block was required to produce the crescent-shaped area of oceanic crust underlying most of the deepwater area of the GOM that was mapped by previous, refraction studies (Ibrahim et al. 1981; Ebeniro et al. 1986) (Fig. 1). While these previous studies all proposed a single pole of opening in the vicinity of western Cuba, Imbert and Philippe (2005) and Pindell and Kennan (2009) proposed a multi-phase episode of seafloor formation based on the observation of extreme asymmetry oceanic crust with 55–60% of the crust located on the northern side of the extinct spreading center (Müller et al. 2008) and NWW–SEE-striking, "pseudo faults" in the eastern GOM. Kleinrock et al. (1977) defined "pseudo faults" to be sets of *en echelon* fracture zones that are frozen into progressively younger crust (Hey 1977), and suggested that they usually represent a propogating spreading center.

Spectrum Geo has acquired and processed an extensive amount of high-quality, 2-D seismic data in the eastern GOM since 2007. In this study, these seismic data—that include the continent-ocean boundaries of the Florida and Yucatan conjugate margins—are integrated with regional gravity and magnetic data to provide a new, detailed, seafloor to Moho interpretation of the extinct, late Jurassic-to earliest Cretaceous mid-ocean ridge and fracture zone system in the deepwater GOM.

Geologic setting of late Jurassic-to-earliest Cretaceous oceanic crust in the eastern Gulf of Mexico

The GOM was formed by late Triassic -late Jurassic, continental rifting and late Jurassic-earliest Cretaceous seafloor spreading (Marton and Buffler 1994; Pindell and Kennan 2009; Hudec et al. 2013; Eddy et al. 2014; Nguyen and Mann 2016) (Fig. 2). The initiation and cessation of oceanic crust formation in the GOM was related to the counterclockwise rotation of the Yucatan block away from North America. However, the exact age of seafloor spreading is not well constrained as high-amplitude continuous magnetic anomalies associated with seafloor spreading have not been well recognized in the GOM. Lack of magnetic anomalies in the GOM is indicative that the GOM oceanic crust was formed during the "Jurassic Magnetic Quiet Zone" (Bird et al. 2005; Christeson et al. 2014).

The location of where the seafloor initiated (COB) in the EGOM is well defined on gravity data, especially along the Yucatan margin (Nguyen and Mann 2016). Free air gravity changes from 20 to −20 mGal within 10 km. The gravity change is less prominent in the Florida side especially under the thick salt found in the northeastern GOM. From the seismic reflection data, the COB is usually interpreted as the "step-up fault" defined by a more depressed, area of thinned, continental crust and a more elevated area of Jurassic, oceanic crust (Hudec et al. 2013).

Four long-offset, wide-angle seismic reflection and refraction profiles were acquired in the Gulf of Mexico Basin Opening (GUMBO) project in an effort to understand the crustal structure and opening history of the GOM (Christeson et al. 2014; Eddy et al. 2014, 2018) (Fig. 1b). Two of the GUMBO profiles in the EGOM traverse the late Jurassic-to-earliest Cretaceous spreading center and allow an estimate for the timing of seafloor accretion based on the stratigraphic ages of the overlying Jurassic and Cretaceous sedimentary units (Snedden et al. 2013, 2014) (Fig. 2). The distance between COB identified from free-air gravity of Sandwell and Smith (2009) and the extinct spreading center recognized from reflection data provide the length of the half spreading. Based on the age of horizons penetrated in the deep-water exploration well LL #399 in EGOM, Snedden et al. (2013) and Eddy et al. (2014) estimated that the seafloor spreading rate along GUMBO 3 was ~2.4 cm/year. To the east along G4, Christeson et al. (2014) and Snedden et al. (2014) calculated a seafloor spreading rate of ~2.2 cm/year. We propose that the lower spreading rate along GUMBO 4 reflects the closer location of GUMBO 4 to the GOM pole of opening near western Cuba (Fig. 1b).

Data and methods

Gravity and magnetic data

The US maritime sector of the study area in the eastern GOM has been regionally surveyed by the Deep East 2D reflection program. Deep East was acquired by the Spectrum-operated, industry seismic vessel GeoArctic in 2007 over a survey area of 120,000 km^2 (Fig. 3a). The shot point interval and time record length for this seismic grid are 37.5 m and 13–14 s, respectively. The seismic data were processed using Kirchhoff pre-stack depth migration (PSDM) commonly used for moderately-complex, geologic settings. The Mexican maritime sector of the study area along the Yucatan margin was surveyed by 2-D reflection data acquired by Spectrum Geo in 2015. These reflection data were made available to us only as two-way travel time sections (Fig. 3b). Gravity and magnetic data were acquired along with these seismic surveys. Open-file potential fields and topography grids were secondary data sources that were integrated as needed into the study (Row et al. 1995; Finn et al. 2001; Sandwell et al. 2014).

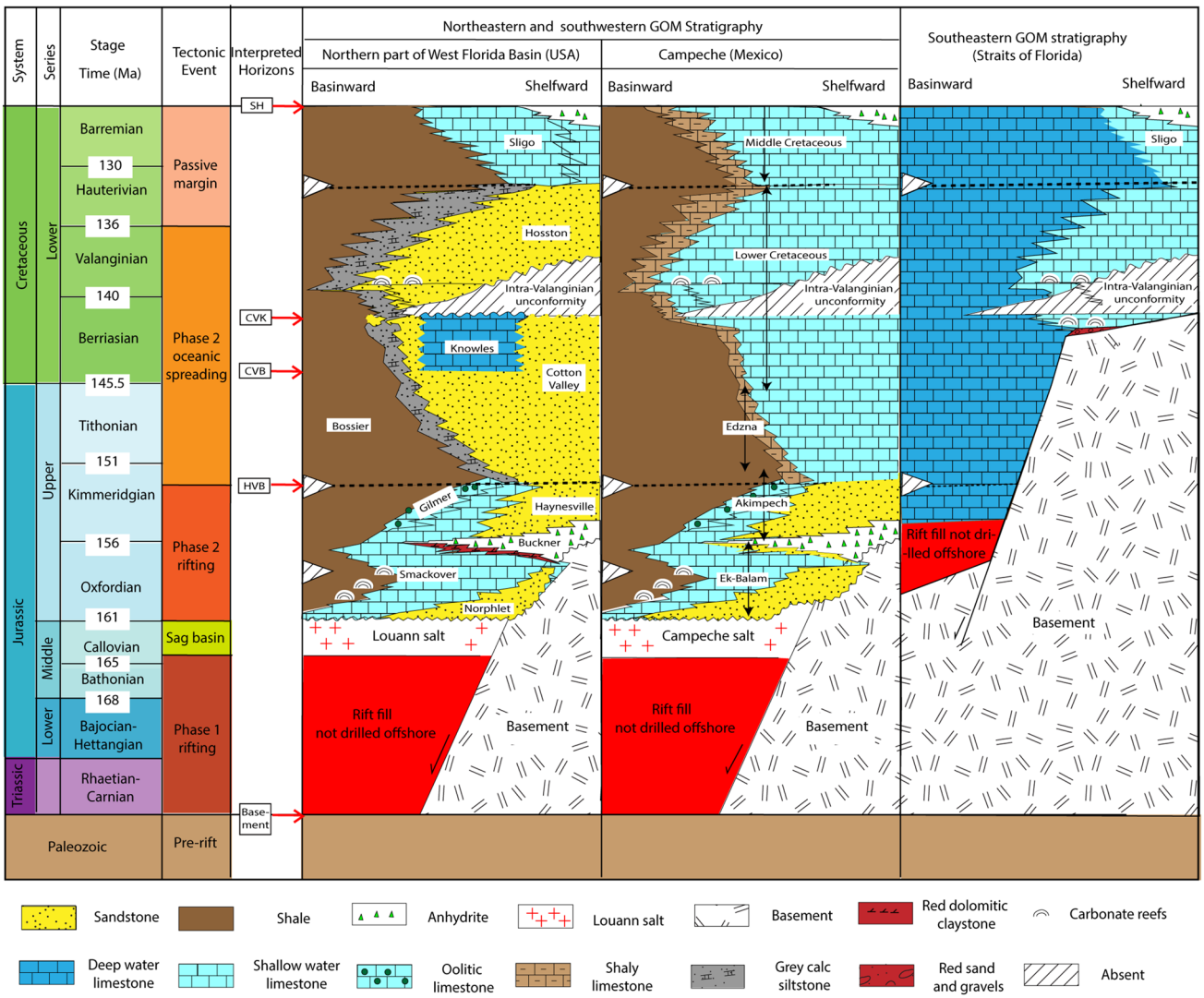

Fig. 2 Stratigraphy of the northeastern and southwestern EGOM correlated with six, tectonic phases for GOM basin history including (1) pre-Triassic, pre-rift phase; (2) Triassic-middle Jurassic Phase 1 rifting; (3) Callovian sag basin (Louann-Campeche salt); (4) Oxfordian-Kimmeridgian Phase 2 rifting; (5) Late Jurassic-early Cretaceous Phase 2 oceanic spreading; and (6) early-late Cretaceous passive margin. The chronostratigraphic columns for the northern part of the West Florida Basin are modified from Dobson and Buffler (1997), Goldhammer and Johnson (2001) and Snedden et al. (2014). The chronostratigraphic column for the Campeche area of Mexico in the southwestern GOM is modified from Ángeles-Aquino and Cantú-Chapa (2001). The chronostratigraphic column for the southeastern GOM stratigraphy is modified from Marton and Buffler (1999). Top of Sligo–Hosston Formations (SH); top of Cotton Valley–Knowles Formations (CVK), top of Cotton Valley–Bossier Formations (CVB) and top of Haynesville Formation (HVB) are horizons interpreted from the grid of 2D seismic data used in this study. Sedimentary fills of rift basins have only been drilled onshore in Florida, Alabama, Mississippi, Arkansas and Texas (Salvador 1991)

Gridded, ship-track potential fields and bathymetric data coverages are displayed in Fig. 1b, 3a, b and 5a. Bouguer gravity anomalies were calculated by assuming the density beneath the water bottom is 2.0 g/cm^3, then 0.97 g/cm^3 density was added for the water layer (Fig. 4a), thus minimizing gravity anomalies produced at the water bottom. Residual Bouguer gravity anomalies were then derived by subtracting a 3-km-upward continuation of Bouguer anomalies from the original Bouguer gravity grid (Fig. 4b). Residual gravity anomalies enhance short wavelengths at the expense of long wavelengths and allow subtle anomalies to be more confidently interpreted. Following Besse and Courtillot's (2002) true polar wander path for the Jurassic age EGOM (140 Ma), we calculated reduced-to-pole magnetic anomalies using paleo-magnetic field inclination and declination values of 48.2° and −24.5°, respectively (Fig. 5b).

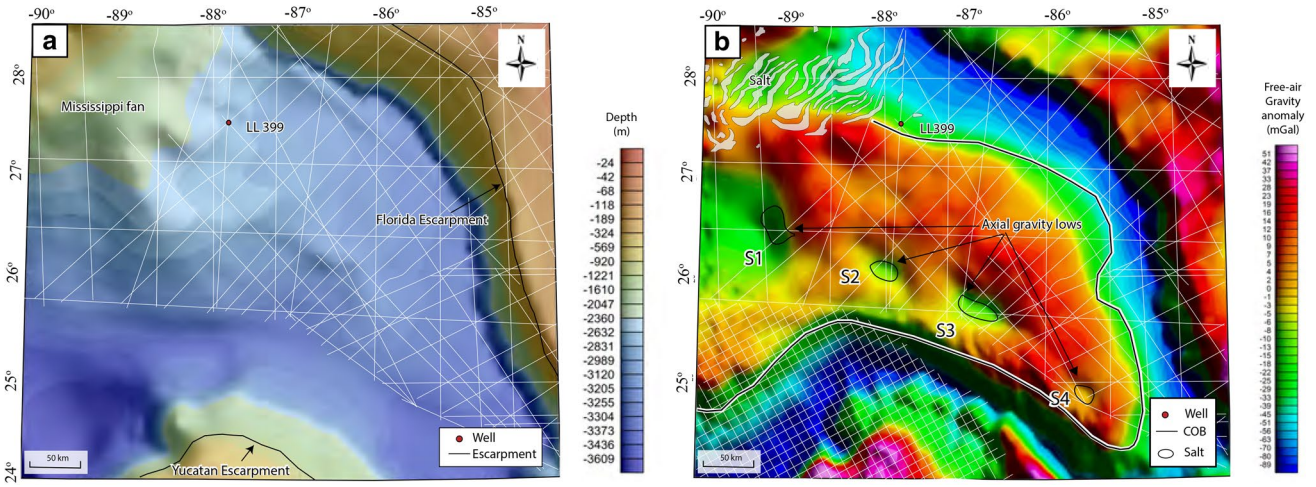

Fig. 3 **a** Bathymetric map for the EGOM study area. Thin, white lines show the locations of 2D seismic reflection lines of the Spectrum Big Wave, 2D seismic reflection data set that was used for mapping the Mesozoic-Cenozoic sedimentary section and late Jurassic-earliest, oceanic crust in the EGOM. All 2D seismic reflection lines of this data set were depth-converted by Spectrum. **b** Ship-based, free-air gravity map of the same area shown in **a**. The pink line is the continent-ocean boundary (COB) identified from the gravity inversion used in this paper to map crustal thickness. The white lines show locations of tracks for ship-based gravity and magnetic data. The subcircular, gravity lows that mark four, extinct, Jurassic spreading ridge segments are labeled S1, S2, S3, and S4

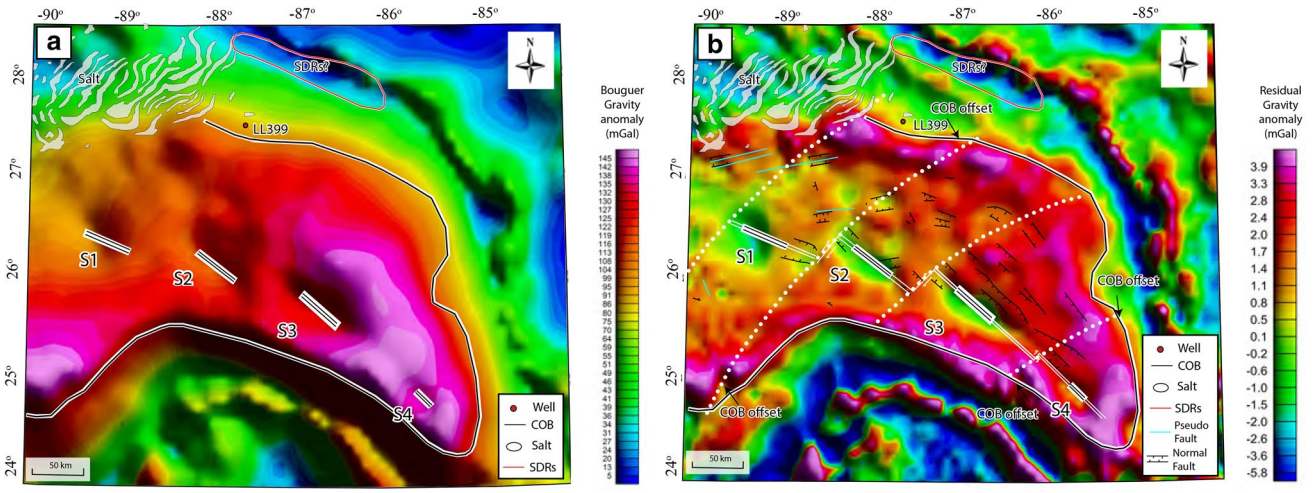

Fig. 4 **a** Bouguer gravity anomalies of the EGOM study area. White bars are locations of inferred relict spreading centers. Red circles represent the potential seaward-dipping reflectors (SDRs?) mapped by Imbert (2005a, b). **b** Residual Bouguer gravity anomalies generated by 3 km upward continuation separation with short, white bars indicating inferred, spreading-ridge segments, and white, dashed lines represent small-circle flow lines about the pole of rotation. Normal faults and areas of major salt bodies mapped from the 2D seismic grid are indicated. Small, black arrows show locations of breaks in linear trends of the Bouguer gravity anomaly along our proposed continent-ocean boundary (COB). These breaks are inferred to represent marginal offsets along the projection of fracture zones into the continental margin

Seismic horizons and well data

Two horizons were interpreted as constraints for the gravity-modeling study: the top of basement and base of the crystalline crust (Moho). Jurassic to Tertiary horizons were correlated throughout the study area and tied to ages identified in the single well LL399 Shell #1, also referred to as "Cheyenne", following chronostratigraphically-defined horizons from Galloway et al. (2000) and Snedden et al. (2013). LL 399#1 with a total depth of 5370 m is the only well drilled into the Jurassic sediments in the deepwater NE GOM in 2004. It was drilled deep into a salt dome located near the salt bounday depositional edge. Mapped horizons tied to the LL399#1 well

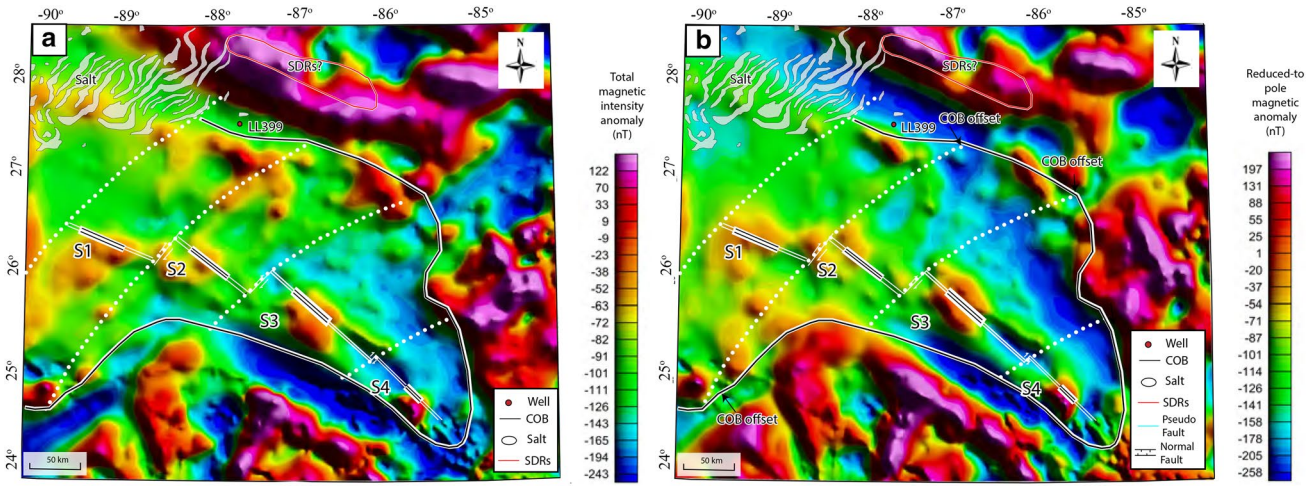

Fig. 5 **a** Total magnetic anomalies of the EGOM study area. Thinner, white bars are the inferred prolongations of spreading ridge (short, white bars) mapped from 2D seismic reflection and gravity data shown in Fig. 4a, b. White, dotted lines are small-circle flowlines calculated from GOM opening pole located by Nguyen and Mann (2016) near northwestern Cuba (22.41°, − 84.33°). **b** Reduced-to-pole magnetic anomalies are shown for the EGOM study area

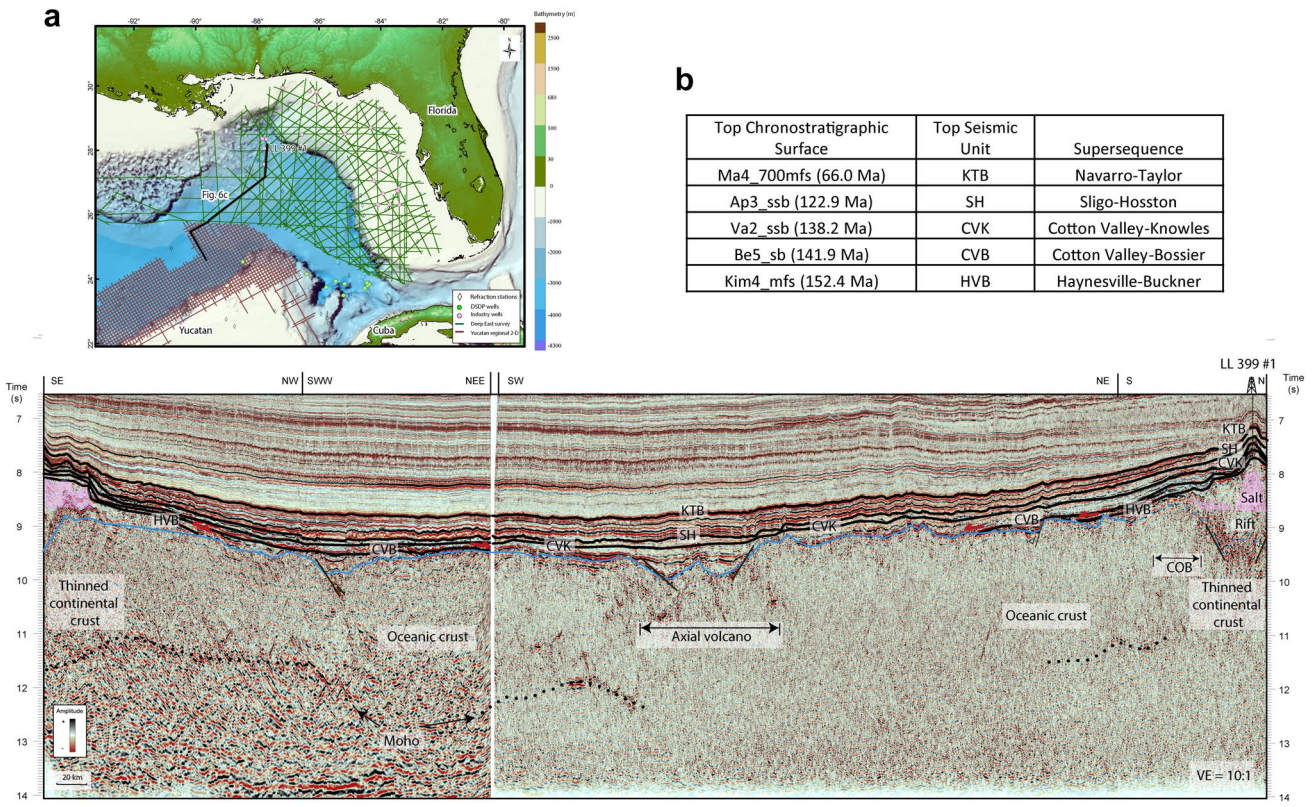

b

Top Chronostratigraphic Surface	Top Seismic Unit	Supersequence
Ma4_700mfs (66.0 Ma)	KTB	Navarro-Taylor
Ap3_ssb (122.9 Ma)	SH	Sligo-Hosston
Va2_ssb (138.2 Ma)	CVK	Cotton Valley-Knowles
Be5_sb (141.9 Ma)	CVB	Cotton Valley-Bossier
Kim4_mfs (152.4 Ma)	HVB	Haynesville-Buckner

Fig. 6 **a** Location map of 2D seismic reflection grids used to correlate features on the conjugate margins of Florida and Yucatan. Heavy lines indicate the location of the 2D seismic reflection lines shown in (**c**). **b** Chronostratigraphy of seismic reflection units are modified from Snedden et al. (2014). **c** 69-km-long, time-migrated seismic section showing correlated seismic sections on the Florida and Yucatan conjugate margins (locations of seismic sections are shown on the map in (**a**)). The blue horizon represents the interpreted top of Jurassic, oceanic basement. Labeled horizons include the following stratigraphic horizons defined by Snedden et al. (2014): Cretaceous–Tertiary boundary (KTB); top of Sligo–Hosston Formations (SH); top of Cotton Valley–Knowles Formations (CVK), top of Cotton Valley–Bossier Formations (CVB) and top of Haynesville Formation (HVB). The black dotted horizon is the interpreted Moho from 2D seismic reflection data

include: the Paleocene-Eocene boundary (PEB) (56 Ma); the Cretaceous–Tertiary boundary (KTB) (66 Ma); the top of Sligo–Hosston (SH) (123.9 Ma); and the top of Cotton Valley–Knowles (CVK) (138.2 Ma) (Fig. 6). We converted the major time horizons from the Yucatan margin to depth horizons using the following velocities: water: 1500 m/s, Tertiary sediments: 2700 m/s, Sligo–-Hosston sediments: 3000 m/s, and sediment older that Hosston: 3400 m/s.

Gravity modeling

The 3-D gravity model includes five layers separated by four horizons: sea surface, bathymetry, basement, and Moho. For the US sector of the EGOM, we interpreted basement and Moho from the grid of Spectrum's Deep East seismic reflection survey. For the Mexican and Cuban sectors of the EGOM, the basement grid was calculated by subtracting NOAA's sediment thickness grid (Whittaker et al. 2013) from the bathymetry. Our initial Moho grid was derived from an isostatic calculation (Blakely 1995).

$$d_m = h\left(\rho_t/\Delta\rho\right) + d_s$$

In this equation, all depths are in km, d_m and ds are the Moho depth with the compensation depth (33 km) at the shoreline, h is elevation, ρ_t is the average crustal density, and $\Delta\rho$ is the density contrast at the base of the crust.

Due to a low, signal-to-noise ratio in the deep portions (below ~ 10 km) of the seismic reflection data, a single velocity of 7 km/s was applied to the depth conversion for these parts of the seismic sections. We adjusted the Moho interpreted from reflection data by 500 m by comparing these deep velocities with seismic refraction velocities (Ibrahim et al. 1981; Christeson et al. 2014; Eddy et al. 2014, 2018). The density of water, crystalline crust, and upper mantle used in our model were 1.03, 2.85, 3.3 g/cm^3, respectively, similar to values used in previous gravity model studies in the GOM (Bird et al. 2005; Nguyen and Mann 2016).

Sedimentary rock densities were gridded as a function of the thickness of the entire section by integrating each grid node over an exponential decay function that simulates clastic compaction of sedimentary rocks (Cordell 1973). Structural inversion of the Moho in our 3-D gravity model was performed using a method described by Parker (1973), which established a Fourier transform technique for calculating potential field anomalies that are produced by uneven layers. The overall survey resolution of gravity data is less than 1 mGal, therefore the inversion convergence limit was set to 1 mGal, which the algorithm achieved after six iterations.

Results

Gravity and magnetic anomalies of the spreading ridge and oceanic crust of the EGOM

Four isolated, circular-to-elliptical, free-air gravity lows with an amplitude of 4 mGal are observed trending northwest-southeast across the eastern GOM (S1–S4 in Fig. 3b). The S1–S4 anomalies comprise more linear NW-SE trending features in the residual Bouguer gravity after subtracting the deeper effect of the Moho (Fig. 4b). The residual gravity map can also be used to interpret faults in the oceanic crust especially in areas of sparse, 2-D seismic data coverage (Fig. 4b). Normal faults shown on the 2D seismic reflection data show a good correlation with subtle and linear, residual gravity lows. Therefore, when we mapped a fault on a single, seismic profile, we can use the residual Bouguer gravity to constrain the fault length. A comparison of the residual gravity map to the location of pseudo faults proposed by Imbert and Philippe (2005) is shown in Fig. 4b. Some gravity signatures are observed along the proposed pseudo faults which may indicate a ridge jump towards northwest.

Basin-opening small circle flowlines, which represent a theoretical pathway for oceanic crust formation, were generated using the pole of rotation proposed by Nguyen and Mann (2016) (Fig. 5a, b).. The flowlines shown on Fig. 5a, b align with (1) apparent offsets of the ridge segment interpreted to be small transform offsets or "secondary discontinuities"; (2) lineaments in the adjacent oceanic crust that also align with the offsets of the ridge; and (3) offsets in the interpreted continent-ocean boundary—such as the flowline between ridge discontinuities S1 and S2 project in the landward direction to align with offsets of the linear, continental margins of Florida and Yucatan (Fig. 5a). Less pronounced, linear offsets are also observed along the flowline separating S3 and S4 (Fig. 5a, b). Similar small, linear offsets of the continent-ocean boundary have been described from other small, obliquely-opening, oceanic basins such as the Woodlark basin of Papua New Guinea (Taylor et al. 1999) and the Okinawa backarc basin (Liu et al. 2017) of the western Pacific Ocean.

In Fig. 7, bold white lines indicate spreading ridge segments. The magnetic anomaly map shows positive anomalies over the parts of the spreading ridge segments (Fig. 5a). Based on 2D seismic data, these anomalies are interpreted to be produced by large elliptical to circular volcanoes (Fig. 7). This correlation is improved by reduced-to-pole correction of the magnetic data (Fig. 5b).

The red outlined areas of figure 7 correspond to seaward-dipping reflectors (SDRs) as mapped by Imbert (2005a, b). Although high-velocity lower crust (HVLC)

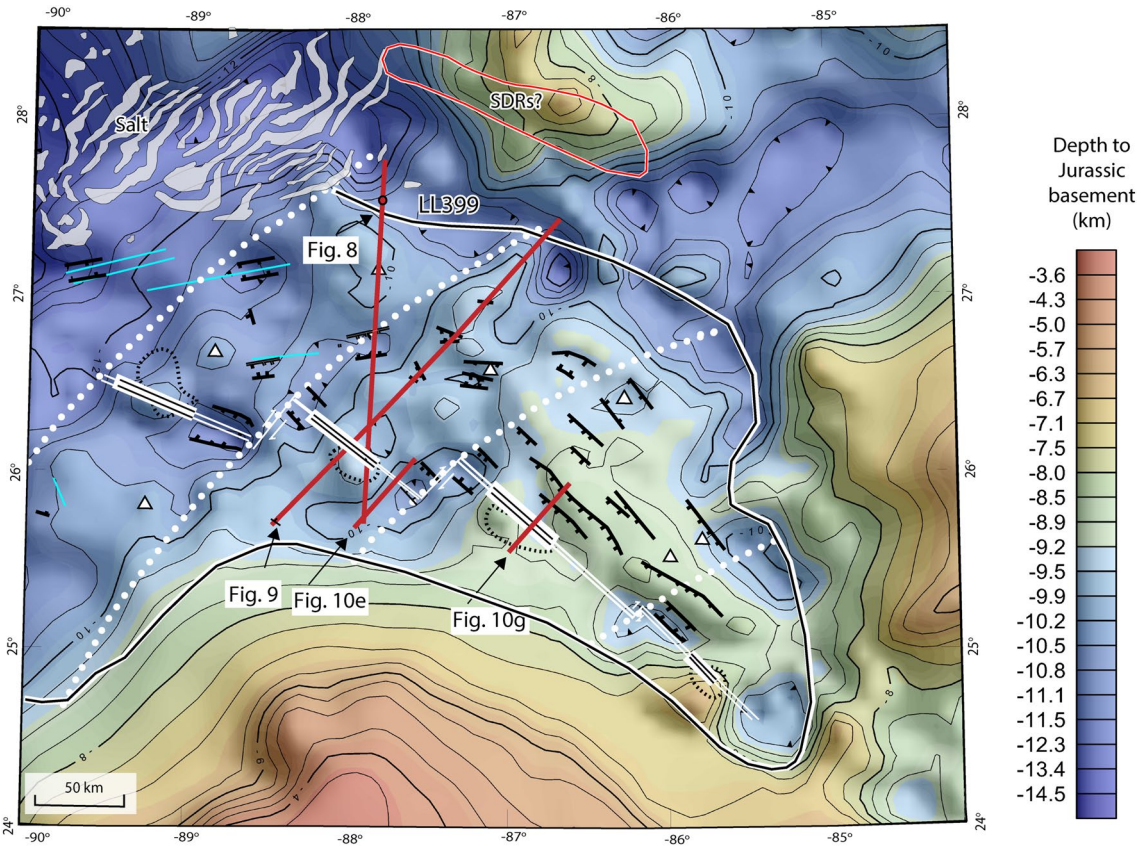

Fig. 7 Structure map with a contour interval of 0.5 km of the top of Jurassic oceanic basement and top of thinned, Paleozoic basement on the Florida and Yucatan conjugate margins interpreted from 2D seismic reflection lines. Map symbols are the same as used in Fig. 4b. Red lines show locations of 2D reflection seismic lines in Figs. 8, 9, 10e, g

beneath these proposed SDRs support a volcanic margin origin for northeastern GOM (Eddy et al. 2014, 2018) (Fig. 7), similar HVLCs and magnetic highs were related to the presence of an inferred, late Paleozoic basin along the same GUMBO 3 line (Lin 2018). Neither the free-air nor residual gravity shows a similar gravity high that might be related to a large area of rift-related, volcanic rocks (Fig. 4). Lin (2018) proposed that the SDRs observed from magnetic and reflection data are more likely related to a late Paleozoic basin with volcanic fill rather than the Mesozoic, rifted margin.

Structure of the oceanic basement in the EGOM

Seismic reflection expression

The top of oceanic basement was defined within our seismic reflection grid as a continuous but rugose high-amplitude reflector that separates Mesozoic sedimentary rocks from underlying oceanic crust (Figs. 8, 9). A series of linear fault-bounded ridges that strike sub-parallel to axial spreading centers are "abyssal hills" commonly observed worldwide on oceanic crust. The top of continental basement was picked at the base of rifted, Mesozoic sedimentary rocks (Fig. 8). The base of salt horizon is picked along a moderate to strong amplitude subhorizontal amplitude event (Fig. 8).

Our interpretation of the top of oceanic basement is based on our integration of seismic reflection and gravity data. Our mapping result shows that the observed northwest-southeast elongated, negative gravity anomalies represent a set of buried northwest-southeast elongated, submarine volcanoes. The volcanoes are located near the center points of the four 30–60-km-long, axial rift valley segments observed in the eastern GOM (Fig. 10). These axial volcanoes show a maximum, vertical relief of 1–2 km within the centers of the ridge segments (labeled as R1 through R4 on Fig. 10)—but decrease in size and elevation towards the ends of each spreading segment.

Examples of axial rift volcanoes that decrease in height and width as they approach the end of spreading ridge are shown on 2D seismic lines in Fig. 10a–e. Ridge axis volcanoes range from 10 to 30 km in width and 1–2 km in height.

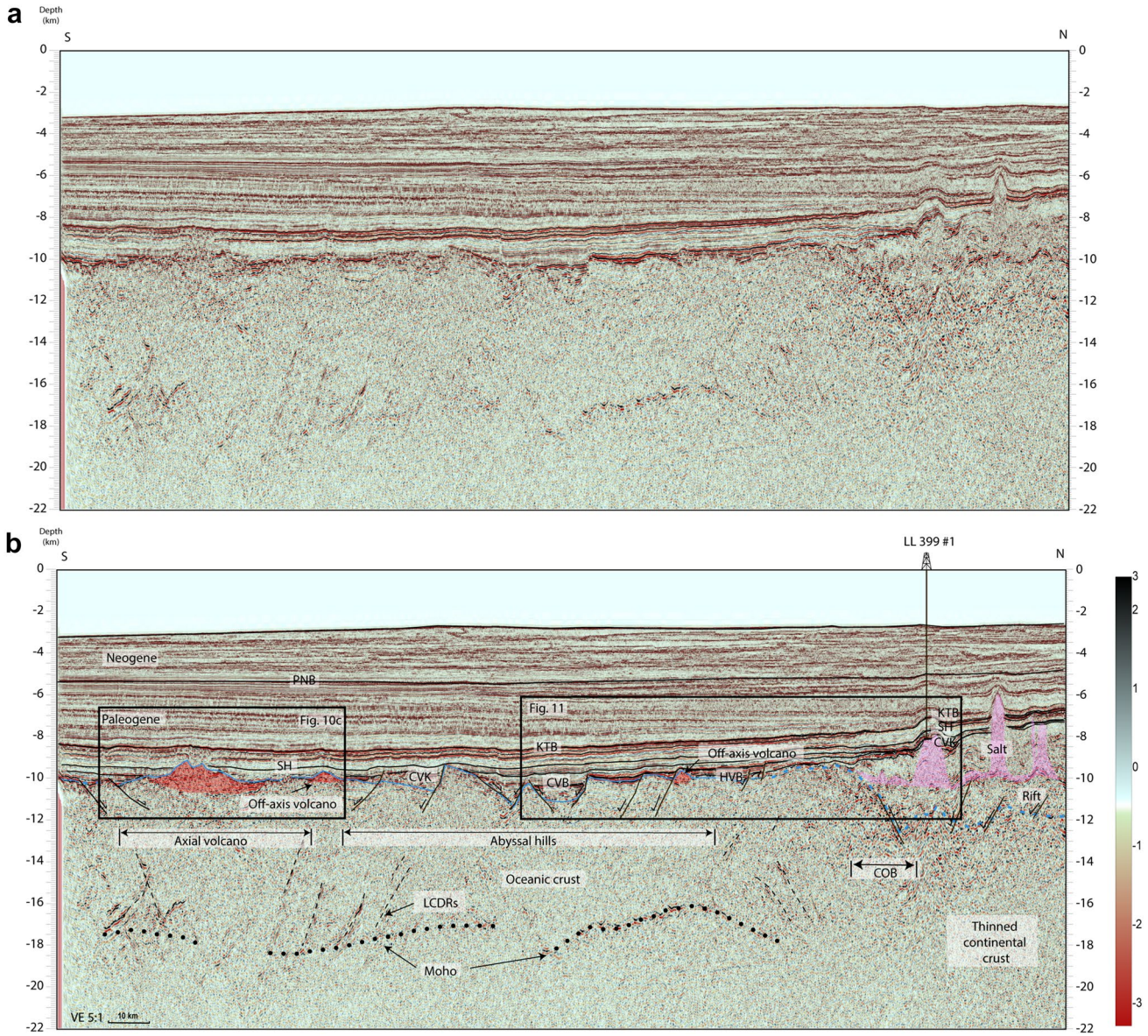

Fig. 8 **a** Uninterpreted depth-migrated 2D seismic line crossing the extinct, late Jurassic-to-earliest Cretaceous spreading ridge, the oceanic crust northeast of the spreading ridge, and the marginal rift marking the continent-ocean boundary along the Florida margin. **b** Interpreted depth-migrated seismic section showing large, late Jurassic volcano occupying the axial valley of the extinct, spreading ridge and rifted late Jurassic-earliest Cretaceous oceanic crust forming abyssal hills relief northeast of the spreading center. Near-vertical black dashed lines indicate lower crustal, dipping reflectors (LCDR) within the oceanic crust. The marginal rift formed on thinned, continental crust and localizes thicker salt deposits. Deep-water, industry well LL-399#1 is located at the crest of one of these salt diapirs and was used by us in this paper and previously by Snedden et al. (2013) to correlate sedimentary formations above late Jurassic, oceanic crust as shown on the stratigraphic columns in Fig. 2. The black rectangle to the left shows a zoomed area of the spreading ridge shown on the 2D seismic reflection line in Fig. 10d. The black rectangle to the right is a zoomed area of the seismic well correlation shown on the 2D seismic reflection line shown in Fig. 11

Wide, axial valleys were mapped where ridges and fracture zones intersect. These features are termed "nodal basins" by Fox and Gallo (1984). The nodal basins increase in length and depth as the pole of rotation is approached; we infer that this lengthening and deepening of the nodal basins to the southeast reflects a slowing of the spreading rate as the pole of rotation is approached.

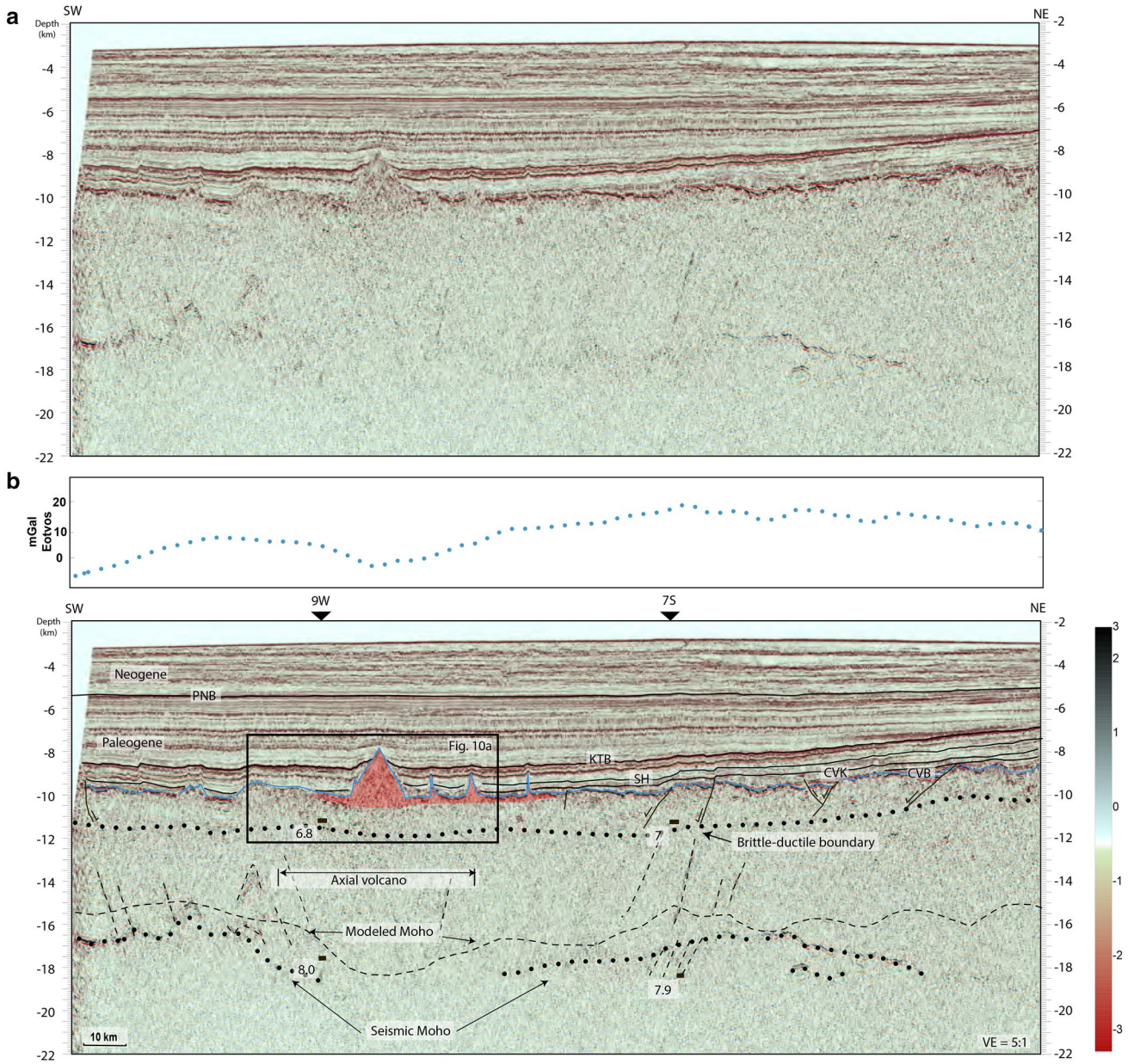

Fig. 9 **a** Uninterpreted depth-migrated seismic section located on the map in Fig. 7 and showing a large volcano occupying the axial valley of spreading segment 2 (this seismic line is located on the map in Fig. 7). **b** Interpreted depth-migrated seismic section with the dotted, grey line showing the brittle-ductile boundary interpreted from the integration of refraction and seismic, reflection data. The dashed black line is the Moho generated in this study from a 3-D gravity inversion. The gravity profile at the top of the seismic line is extracted from the free-air gravity grid shown in Fig. 3b

Expression of secondary discontinuities along the ridge axis

Slow-spreading centers are characterized by different scales of discontinuity gaps. A first-order discontinuity is a transform fault that connects spreading centers offset by as much as several hundred kilometers (Fox and Gallo 1984). Secondary discontinuities are less well developed and exhibit much shorter (20–80 km) ridge offsets (Macdonald et al. 1993). Globally, fracture zones along active and extinct ridges range in width from 20 to 50 km, but those GOM fracture zones described by Stephens (2001) using 3D seismic data in the northeast of this study area are less than 5 km wide.

In our study area, 30–60 km long ridge segments are separated by 5–30 km inter-volcanic gaps that we interpret as second-order discontinuities as defined by Macdonald et al. (1993) (Fig. 7). We extended the interpreted ridge segments

marked by the residual gravity lows as defining the extinct ridge and fracture zone geometry of the EGOM (Fig. 7).

Small-circle flowlines through the proposed fracture zone locations were generated using Nguyen and Mann's (2016) pole of rotation for the Yucatan block. These flowlines roughly correlate with broad, arcuate gravity lows (Fig. 4b), that we infer are the four main spreading segments developed in the EGOM as the late Jurassic-earliest Cretaceous, oceanic basin began to open. Several map view offsets of the edge of the continent-ocean boundary on both conjugate margins coincide with flowline intersections with the continental margins and are inferred to represent the earliest accretion of oceanic crust along the continent-ocean boundary (Figs. 4, 5).

Structural and volcanic features of the ridge axis and adjacent oceanic crust

The overall basement fabric of the study area consists of northwest-trending basement faults that dip towards the extinct spreading center, as is commonly observed along active slow-spreading ridges (Fox and Gallo 1984) (Fig. 7). These normal faults have relatively small offsets that vary from 0.2 to 1 km (Fig. 9). In the north-trending, regional 2D seismic line that intersects deep-water, well LL 399, a 15-km-wide 2-km-deep valley is bounded by east–west striking and inwardly-dipping normal faults (Fig. 8). These basement faults follow the general trend of pseudo faults previously proposed by Imbert and Philippe (2005) in the northeastern EGOM (Fig. 7). However, we interpret these features as transform fault valleys that parallel the flow-line parallel fracture zones.

In addition to the large volcanoes located in the centers of spreading segments, off-axis volcanoes are widely distributed on the Jurassic oceanic crust that flank the spreading ridge (Fig. 7). Several of these off-axis volcanoes formed either near oceanic basement faults or within basement depressions.

Seismic reflection data through ridge segment 2 images the largest buried volcano in the study area that is surrounded by several smaller volcanoes (Fig. 9). This central large buried volcano rises 2.2 km above the surrounding basement and is 13.5 km wide with slopes up to ~ 12°. Cretaceous to Tertiary, post-spreading strata onlap these volcanic edifices. The overlying sediments are deformed by differential compaction over the volcanoes. Based on the horizon correlated from well 399 #1, we suggest that the peak of the 2-km-high volcano in this ridge center was not completely buried by overlying Cretaceous and Cenozoic sedimentary rocks until the Late Oligocene (Fig. 9).

Minor extensional normal faults and compaction folds on and above the crest of the ridge volcano are shown in Fig. 10. Sediment horizons below the axial volcanoes in Fig. 3e, g indicate that the volcanic topography formed during the final stages—or immediately after—the end of seafloor spreading. Constraints on the timing of seafloor spreading will be discussed in the next section.

Age of oceanic crust in the EGOM

Based on the horizons correlated from well LL399 #1, the termination of the mapped horizons on the oceanic crust records the opening history of the late Jurassic-earliest Cretaceous GOM (Figs. 11, 12). The lateral extent of the structure maps on both conjugate margins of Florida and Yucatan, mark the progressively widening area of oceanic crust in the EGOM (Fig. 12a–c). The abyssal hill geometry of the surface formed by volcanic-related, basement highs along the spreading ridge controlled the localized, irregularities of the Cretaceous isopachs (Fig. 12d, e). The plate model and ages of oceanic crust are identical to those proposed by Snedden et al. (2013) (Fig. 12f).

The extent of Haynesville deposited the northern flank of the spreading ridge is much wider than the extent of Haynesville on the southern side of the ridge. This observation suggests a ridge jump occurred during Haynesville deposition, as asymmetrical seafloor has only been recognized in about 5% of the world's ocean basins (Müller et al. 2008). Based on the pseudo faults and salt limit in the northeastern GOM, Imbert and Philippe (2005) and Pindell et al. (2009, 2016) proposed an early stage of near northeast-southwest seafloor spreading in the oceanic crust that was accompanied by thinner deposition of Jurassic salt than the central GOM. Our mapping of Jurassic and Cretaceous, sedimentary horizons and isopach maps suggests a poorly-defined, northwest-southeast spreading ridge northeast of the single, pole of rotation in northwest Cuba. The inferred ridge is shown as a black, dashed line on the map in Fig. 12f.

The morphological expression of extinct, spreading ridges have been described from other oceanic basins, such as from the Mathematician ridge that formed in the Pliocene (4 Ma) in the eastern equatorial Pacific (Mammerickx et al. 1988). This extinct ridge is marked by linear troughs formed during rapid, thermal subsidence following a ridge jump that is recorded by magnetic anomalies (Mammerickx and Sandwell 1986). In this study, the lack of magnetic anomalies combined with deep burial following the cessation of late Jurassic-earliest Cretaceous spreading makes it difficult to identify the exact location of the proposed abandoned ridge in the northeastern GOM.

Inferring age of oceanic crust and subsidence history from patterns of regional, sedimentary isopachs

Jurassic-Cretaceous sediment thickness variations from isopach maps in the Florida and Yucatan margins (Fig. 13)

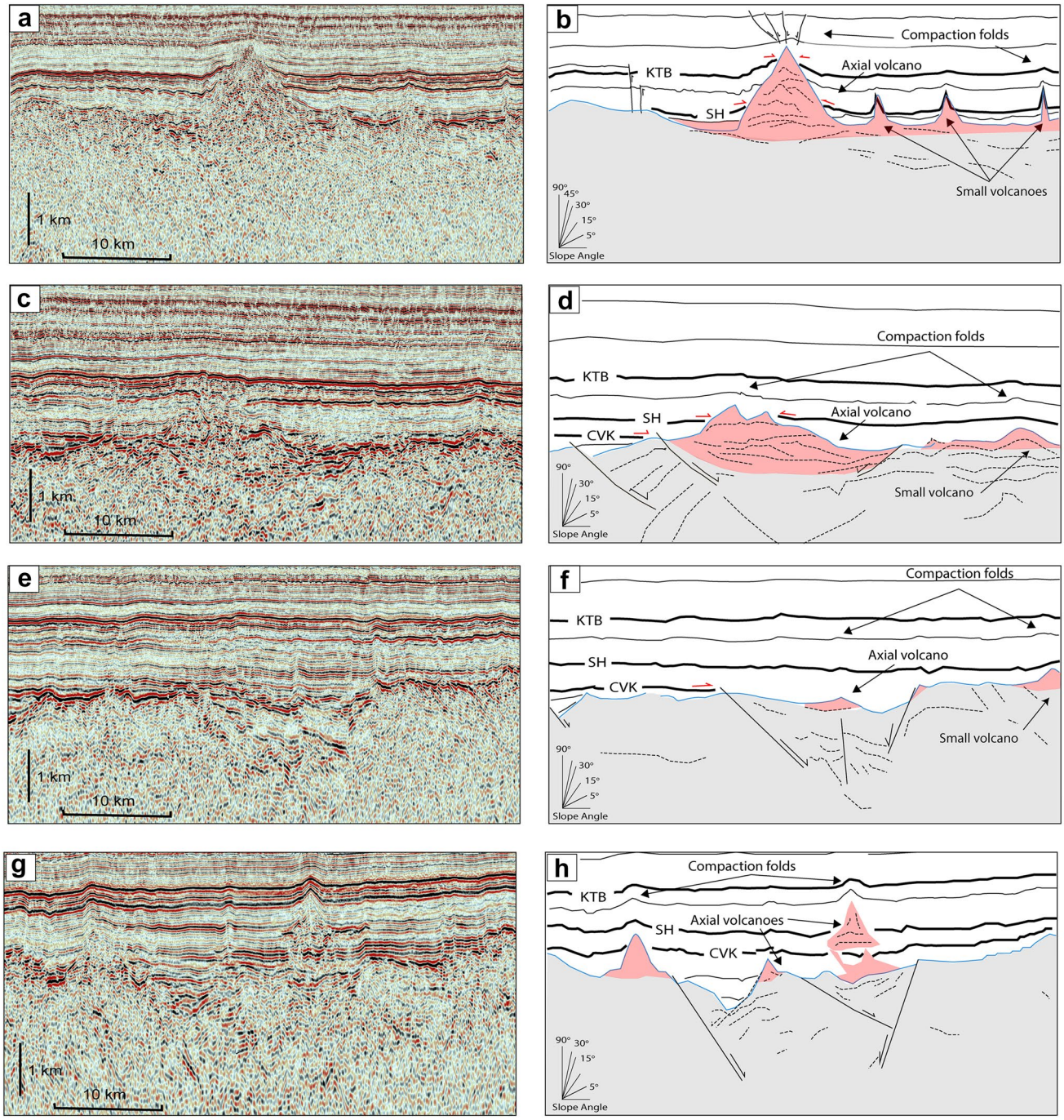

are mainly controlled by the combined effects of oceanic basement structure and Mesozoic-Cenozoic sediment supply. In the Kimmeridgian, a thin Haynesville sequence (200–600 m) was deposited on the V-shaped area of oceanic crust in the northeastern GOM (Fig. 13a). In the Tithonian, a 1000–1300 m thick Cotton-Valley-Bossier fluvial-deltaic sequence was deposited on the newly-formed, oceanic crust in the southeast, with clastic, sedimentary sources created by continental rifting processes that accompanied ridge propagation into the southeastern GOM (Marton and Buffler 1999) (Fig. 13b).

In the Berriasian, the oceanic crust finally achieved its maximum extent and present-day geometry as rifting in the southeastern GOM ceased (Marton 1995; Marton and Buffler 1999). The Knowles limestone was deposited following a short transgression near the end of Cotton Valley deposition (Cregg and Ahr 1984; Dobson and Buffler 1997). The Cotton Valley sequence is observed to be thickest (1000–1300 m) within the nodal basins at the ends of spreading ridges and

◂**Fig. 10** **a** Uninterpreted depth-migrated seismic sections across the center of mid-ocean ridge segment 2 (S2). Seismic line locations are shown in Figs. 7 and 9. The axial volcano has 2 km of vertical relief. **b** Schematic illustration of the crustal structure of the spreading ridge and its orthogonal, secondary discontinuities based on the interpretation of the seismic reflection line in Figs. 3, 10a. Folds and minor faults are inferred to form as compaction effects over the top of the large, axial volcanoes. Black lines show more prominent reflectors within Mesozoic-Cenozoic sedimentary units. Bold black lines are horizons identified in Fig. 6b. The black, dashed lines show internal reflectors within the volcano and other, weak reflectors within the upper, oceanic crust. **c** Uninterpreted depth-migrated seismic section 15 km southeast of the line shown in Figs. 3, 10a. Location of seismic line is shown on Figs. 7 and 8. The vertical relief of the axial volcano decreases in this area to less than 1 km. **d** Schematic illustration interpreted from the seismic line in Fig. 10c. As the vertical relief on the axial volcano diminishes, the axial valley marking the Jurassic spreading ridge becomes more pronounced. **e** Uninterpreted, depth-migrated seismic section across the southeastern end of the late Jurassic-to-earliest Cretaceous mid-ocean ridge segment 2 (S2). Location of this 2D seismic section is shown in Fig. 7. The spreading ridge is well defined in this area by a 1-km-deep axial valley, although a series of smaller volcanoes are also visible on the same, seismic section. **f** Interpretation of the 2D seismic line in Fig. 10e. Near the end of ridge segment, the axial valley becomes more prominent. A small volcano overlies sedimentary fill of the axial valley. **g** Uninterpreted depth-migrated seismic section located on Fig. 7 showing ridge segment 3 (S3) with volcanoes adjacent to the axial valley. **h** Interpretation of the 2D seismic line in Fig. 10f. Note that the base of the volcano adjacent to the axial valley overlies the top of Cotton Valley–Knowles Formation as also observed on the 2D seismic lines in Fig. 10d, f. Deposition of the Berriasian Cotton Valley Formation marked the end of late Jurassic-to-earliest Cretaceous seafloor spreading in the age range of 141.9-138.2 Ma

thins onto the axial volcanoes along the spreading ridge (Fig. 13c). In the Valanginian-Barremian, Sligo–Hosston sequence sediments buried most of the structural relief on the oceanic crust—with the exception of the 1–2-km-high, axial volcanoes (Fig. 13d). In the Aptian-Maastrichtian, the Navarro–Taylor sequence was uniformly distributed with its thickest area (1000–1200 m) located in the northeastern GOM (Fig. 13e).

Tertiary, clastic sediments are 7600 m thick in the northeastern part of EGOM, and thin to 2000 m in the southeast part of EGOM (Fig. 13f). From Kimmeridgian to Maastrichtian, relatively thinner (1000–1500 m) Late Jurassic deepwater sediments were deposited on the Yucatan margin compared to the Florida conjugate margin (2000–2500 m) (Fig. 13a–e). The 1000–1300-m thick Haynesville, Cotton Valley–Bossier sequences were deposited during seafloor spreading in the southeastern EGOM (Fig. 13a–c) and represent the inferred combined effects of: (1) a slowing spreading rate in this location closer to the pole of rotation in northwestern Cuba; and (2) the proximity to terrigenous, clastic sources in southeastern EGOM (Escalona and Yang 2013).

The 800–1000-m-thick Cotton Valley–Knowles and 600–1000-m Sligo–Hosston sequences in the northeastern part of the EGOM both reflect a rapidly subsiding oceanic crust following the cessation of seafloor spreading around Berriasian time (Fig. 13d, e). Thick Tertiary sediments in the northwestern EGOM were derived from fluvial systems along GOM coastal plain (Galloway 2008). Thin (1000–1500 m) Kimmeridgian to Maastrichtian sediments deposition are related to the lack of fluvial sources along the Yucatan margin.

Crustal structure of oceanic crust of the EGOM

Depth to the Moho from 3D gravity inversion

The seismic Moho beneath the extinct spreading ridge (Fig. 14) was interpreted as a set of deep, high-amplitude, continuous seismic reflectors underlying oceanic basement. The 1–2 km difference in depth between the Moho interpreted from seismic data, and the Moho derived from gravity inversion (Fig. 9) is attributed to the single velocity (7 km/s) used for depth conversion by Spectrum for sub-basement crust. Oceanic crust and upper mantle velocities vary: ~ 4.55 km/s for thin upper crust (Layer 2), ~ 7.1 for lower crust (Layer 3), and > 7.6 km/s for upper mantle (White 2012). The Moho inverted from integrated 3-D gravity inversion reveals the deep root of the Moho underlying the extinct ridge (Fig. 15a). The RMS difference between observed and calculated gravity after the inversion is less than 1 mGal for the oceanic crust, and ± 6 mGal in the region near the continent-ocean boundary (COB) and within the carbonate bank on the Yucatan conjugate margin (Fig. 15b). The average thickness of the oceanic crust derived from the basement and modeled Moho of the EGOM is 6.1 km (Fig. 16). Thicker oceanic crust (> 8 km) was observed in northwestern EGOM along GUMBO3 (Eddy et al. 2014), and normal thickness oceanic crust (5.6–5.7 km) in eastern EGOM along GUMBO4 (Christeson et al. 2014). Modeling results indicate less difference between the northwestern and southeastern EGOM ocean floor. These smaller differences in the two areas of the EGOM could be caused by the high velocity layer under the oceanic crust observed along GUMBO3, which reduces the thickness of the oceanic crust in the northwestern GOM when we modeled the oceanic crust with same density for both northwestern and southeastern EGOM.

Origin of lower-crustal dipping reflectors

Lower-crustal, dipping reflectors (LCDRs) observed in the upper and lower, oceanic crust in areas of fast spreading centers are thought to be related to either: (1)

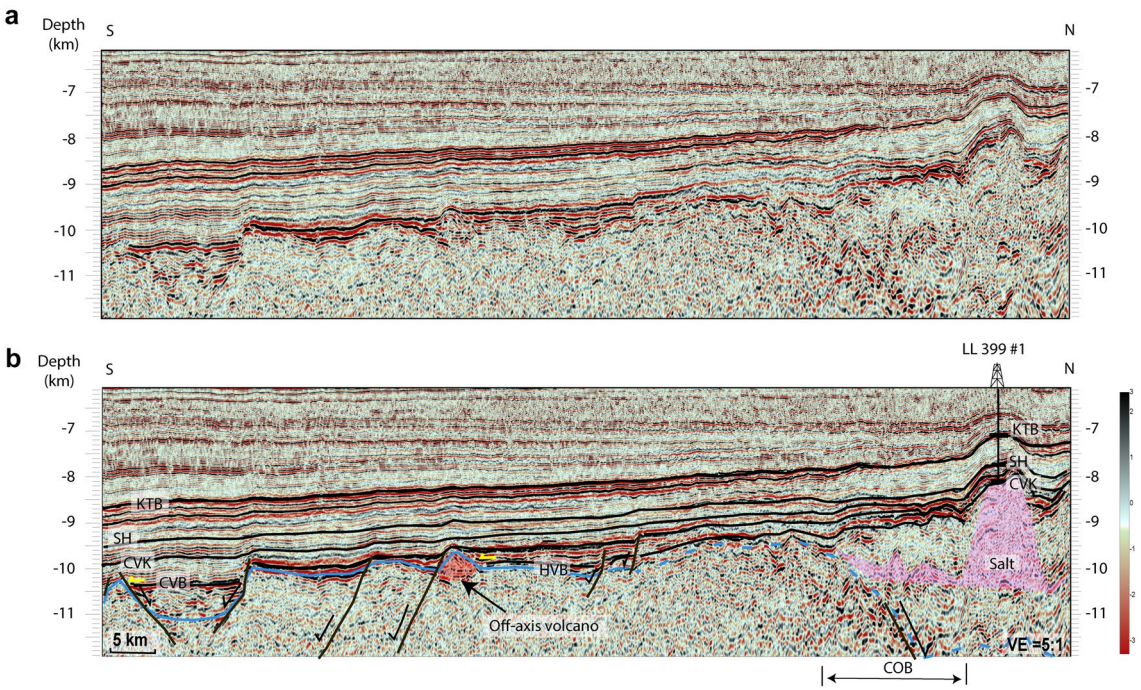

Fig. 11 **a** Zoom of the seismic reflection line shown in Fig. 8a. **b** Zoom of the seismic line shown in Fig. 8b to show the seismic well correlation from deep-water, industry well LL 399 #1 around COB to the oceanic crust in the EGOM study area. Yellow arrows show the onlap onto the top of oceanic crust of the CVB and HVB stratigraphic formations as correlated from well LL 399 #1

hydrothermal circulation at the base of sheeted dikes (Ranero et al. 1997b); or (2) shear zones characterized by interstitial melt or mylontization (Bécel et al. 2015). For slow-spreading ridges, LCDRs observed in other, oceanic basins have been interpreted as: (1) thermal changes caused either by variable spreading rates or the presence of a mantle plume (Ranero et al. 1997a); (2) fault systems that penetrate the entire thickness of oceanic crust (White et al. 1990; Morris et al. 1992); and (3) shear zones related to brittle-ductile deformation (Mutter and Karson 1992).

Based on the relationship between maximum displacement and fault length by (Schultz et al. 2006), small-displacement normal faults with offsets in the oceanic crusr of tens to hundreds of meters do not support the second interpretation that reflectors are fault-plane reflections of normal faults that penetrate the entire lower crust (Figs. 8, 9). We propose that these small-offset, normal faults support the third model proposed above by Mutter and Karson (1992) and reflect deformation of the brittle upper crust by normal faulting during slow, seafloor spreading and deformation of the lower crust along ductile shear zones. The boundary of brittle-ductile deformation correlates with a refraction boundary where velocities increase from 6.3 to 7.0 km/sec (Ibrahim et al. 1981) (Figs. 3, 9).

Discussion

Possible mechanism for gravity lows and magnetic highs observed along an extinct mid-ocean ridge

The axial gravity low observed over active, slow-spreading ridges is generally attributed to partial melting beneath the spreading axis (Jonas et al. 1991). For extinct, slow-spreading ridges, Hall et al. (1986) proposed that the density of the upper mantle was altered during this final phase of upwelling along the spreading ridge and became preserved in place as long-lived, low-density serpentinized bodies. Low, P-wave velocities observed in the upper mantle of other, extinct, slow-spreading ridges (e.g. Labrador Sea – Osler and Louden 1995) support the presence of a low-density, serpentinized mantle root beneath extinct, spreading ridges. We attribute the presence of an axial negative gravity anomaly in the EGOM to the presence of a preserved, low-density mantle root that formed during late Jurassic-earliest Cretaceous GOM seafloor spreading.

For extinct slow-spreading ridges, the axial valley depth and the length of the low-density root are assumed to decrease as the spreading velocity increases (Hall et al. 1986). Therefore, the magnitude of negative gravity anomalies would also tend to decrease as the spreading rate increases. The residual gravity anomaly in the eastern GOM becomes a more linear feature after the effect of the deeper

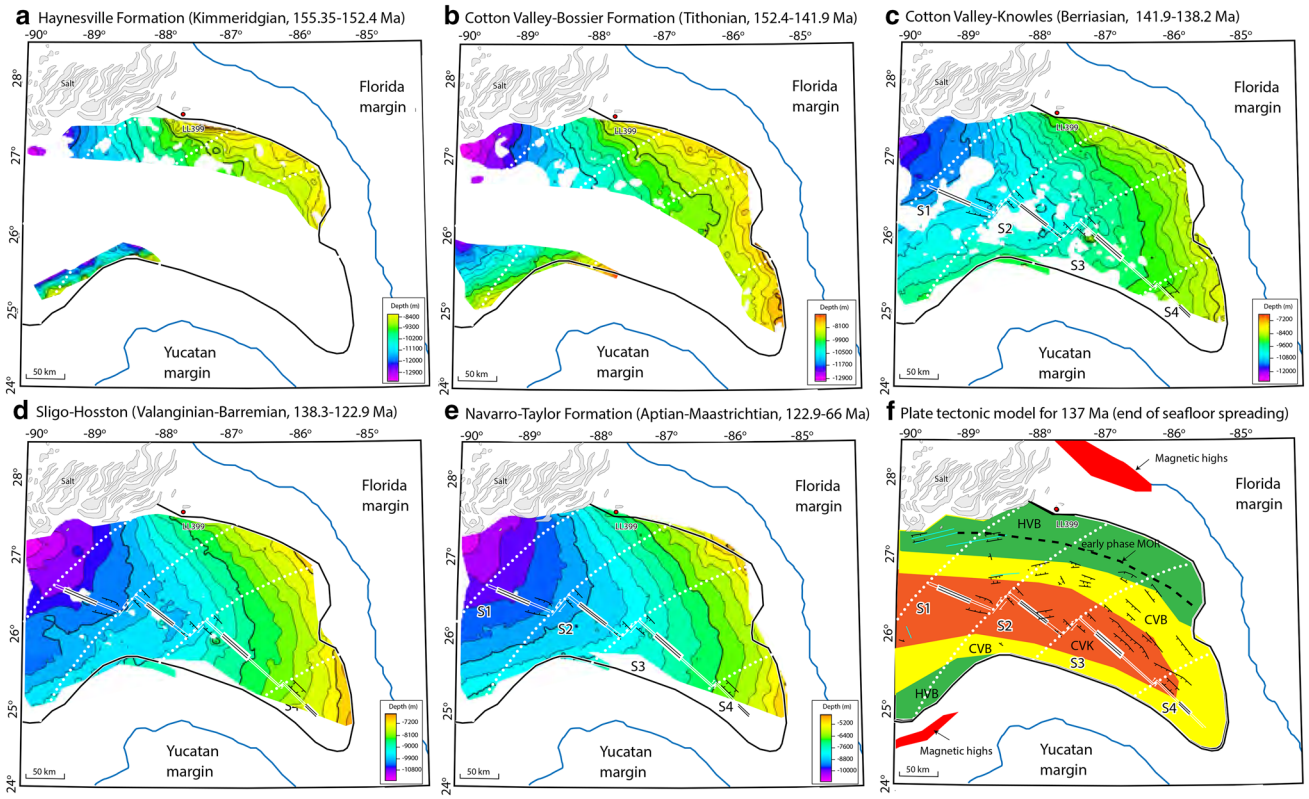

Fig. 12 **a** Structural map in depth of the top of Haynesville Formation (HVB) of Kimmeridgian age (155.35–152.4 Ma). During this period, the oceanic crust was beginning to form along the northeastern and southwestern edges of the EGOM. **b** Structural map in depth of the top of Cotton Valley–Bossier Formation (CVB) of Tithonian age (152.4–141.9 Ma). During this period, the newly-formed, oceanic crust increased the width of northeastern and southwestern EGOM and extended towards the southeast. **c** Structural map in depth of the top of Cotton Valley–Knowles Formation (CVK) of Berriasian age (141.9–138.2 Ma). During this period, oceanic spreading ceased and the present-day width of the oceanic crust was attained. **d** Structural map in depth of the top of Sligo–Hosston Formation (SH) of Valanginian-Barremian age (138.3–122.9 Ma). The top of Sligo–Hosston Formation is the first stratigraphic horizon to bury most of the GOM Jurassic oceanic crust with the exception of several, prominent seamounts aligned along the extinct, spreading axis. **e** Structural map in depth of the top of the Cretaceous–Tertiary boundary (KTB). The Cretaceous–Tertiary boundary is a widespread, unconformity identified in many areas of the GOM (Ibrahim et al. 1981). **f** Plate tectonic model for 137 Ma (end of seafloor spreading) based on compiling the lateral extents of the of the top of Haynesville Formation (HVB), top of Cotton Valley–Bossier Formation (CVB) and top of Cotton Valley–Knowles Formation (CVK) as shown on Fig. 12a-c

part of low-density root centered on the spreading ridge is removed (Fig. 4b).

Different from other slow spreading ridges characterized by axial valleys, the mid-ocean-ridge in the EGOM is expressed as an alignment of axial volcanoes. From seismic profiles across spreading ridge segments of the EGOM which display less volcanism, volcanoes are observed to occur with the axial valley (Figs. 10d, f, h, 17a). Correlating with sediments deposited on the top of the oceanic crust, axial volcanoes were formed after CVK deposited which is around the end of seafloor spreading (Fig. 17b). Post-drift sediments overlying the volcanoes crest were deformed by the differential compaction when the sediments continued to deposit though Cretaceous and Tertiary (Fig. 17c). By the end of Cretaceous, most of the ridge crests were buried by post-drift sediments (Fig. 10).

Volcanism in the spreading center could be related to an underlying, fertile mantle that erupted as the spreading rate decreased—or soon after seafloor spreading had ceased (Haase et al. 2011; Barckhausen et al. 2014). Similar post-spreading volcanism has been observed along an extinct Oligocene spreading center in the South China Sea (Zhao et al. 2016). In the GOM, even the seafloor spreading locked up, the connection to asthenosphere was still active. The fertile mantle built volcanoes at the last gasp or after seafloor spreading terminated along the relict ridges. These large, axial ridge volcanoes are the likely origin for the localized magnetic anomaly highs that were noted by previous studies along the spreading ridge segments in the EGOM (Hall and Najmuddin 1994; Imbert and Philippe 2005; Nguyen and Mann 2016).

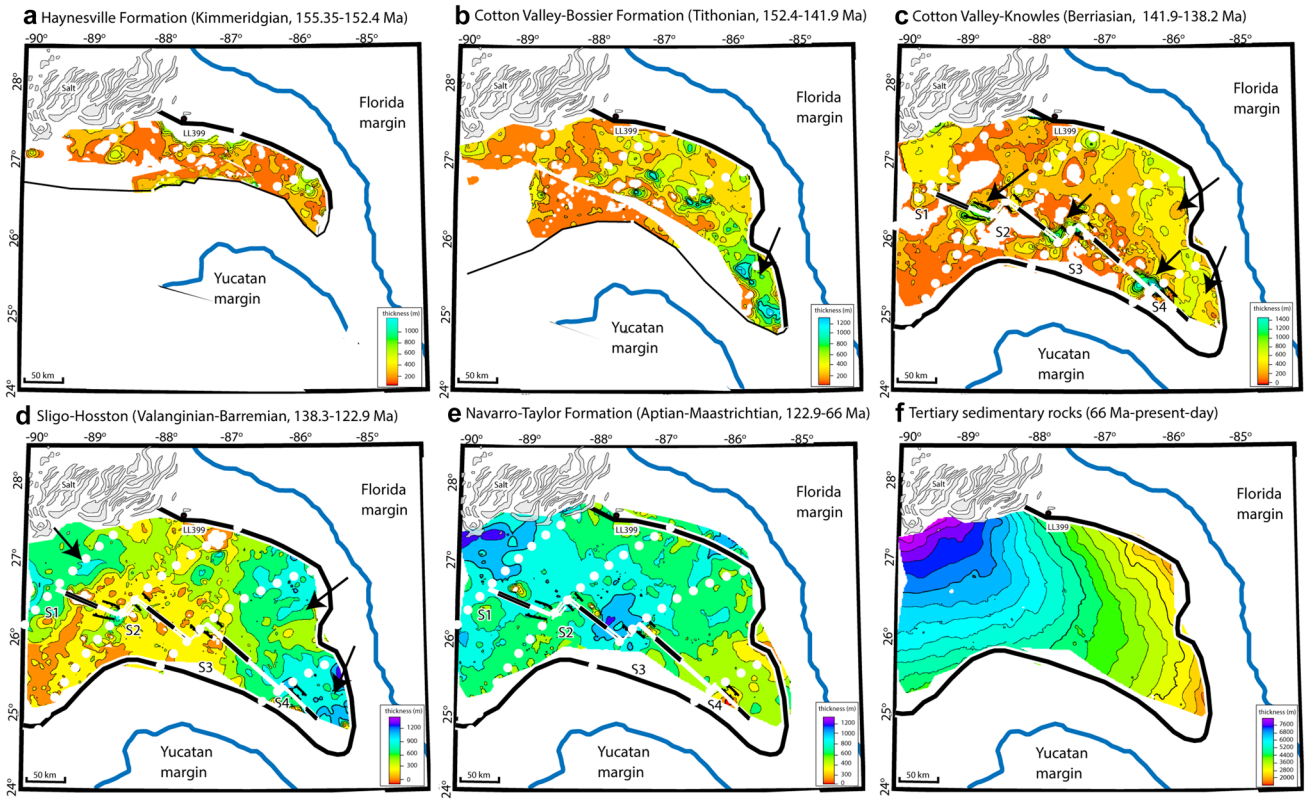

Fig. 13 **a** Isopach map for the late Kimmeridgian stratigraphic interval (155.35–152.4 Ma) between the top of Jurassic oceanic basement and the top of Haynesville (HVB). Reconstructed map bases shown in Fig. 13a–c are all based on the pole of rotation in northwestern Cuba by Nguyen and Mann (2016). **b** Isopach map of the Cotton Valley–Bossier Formation (CVB) of Tithonian age (152.4–141.9 Ma). Black arrow shows a prominent CVB depocenter located in the southeastern GOM. **c** Isopach map of the Cotton Valley–Knowles Formation (CVK) during the Berriasian (141.9–138.2 Ma). Note that the CVK depocenter extends in a northwesterly direction. Thicker sediments were deposited in nodal basins along the spreading center. Black arrows represent the direction of sedimentary infilling. **d** Isopach map of the Sligo–Hosston Formation (SH) of Valanginian-Barremian age (138.3–122.9 Ma). As seafloor spreading ceases, the Jurassic-Cretaceous sedimentary section is evenly distributed in the EGOM with the thinnest sediments occurring along the extinct, ridge axis. **e** Isopach map of the Navarro–Taylor Formation (NT) of Aptian-Maastrichtian (122.9–66 Ma) between the top of Sligo–Housston Formation (SH) and the Cretaceous–Tertiary boundary (KTB) (65 Ma). The thickness of between SH and KTB show abrupt thickness changes along the same trends as the small circles and inferred, secondary discontinuities about the pole in northwestern Cuba. **f** Isopach map of the Tertiary passive margin stage. The rapid thickness increase towards the northwest reflects the southward progradation of the Mississippi fan especially during the period of Miocene to Recent

Possible explanations for crustal asymmetry in the eastern GOM

A possible tectonic mechanism for the asymmetry of the oceanic crust in the eastern GOM was proposed by Müller et al. (2008). He noted that areas of asymmetrical oceanic crust are commonly related to asthenospheric flow from mantle plumes that result in ridge jumps (Table 1). A late Jurassic mantle plume (150 Ma) in the central GOM identified from basement and gravity highs (Bird et al. 2005) may have provided the mechanism for the westward jump of the spreading ridge in the early stage of seafloor spreading (Fig. 18). Another well-studied plume, the Central Atlantic Magmatic Province (CAMP), is believed to have triggered the late Triassic breakup of Pangea which resulted in the Phase 1, NE-SW trending rifts in the central GOM (May 1971) (Fig. 18a). In the late Jurassic, counterclockwise rotation of the Yucatan block led to rifting and seafloor spreading in the GOM (Fig. 18c). The initial spreading center is located on the heavily rifted area in the central and northeastern GOM as shown in our map in Fig. 13a. In the early stage of seafloor spreading around 150 Ma, the presence of late Jurassic mantle plume in the central GOM led to asthenospheric flow from the hotspot and mantle plumes to the early spreading ridge and promoted the southwestward ridge jump towards central GOM (Müller et al. 2008) (Fig. 18c). As the pseudo faults are *en echelon* sets of fracture zones frozen into progressively younger crust (Hey 1977), the WSW-ENE-trending "pseudo faults" also indicate a southwestward ridge jump towards the central GOM.

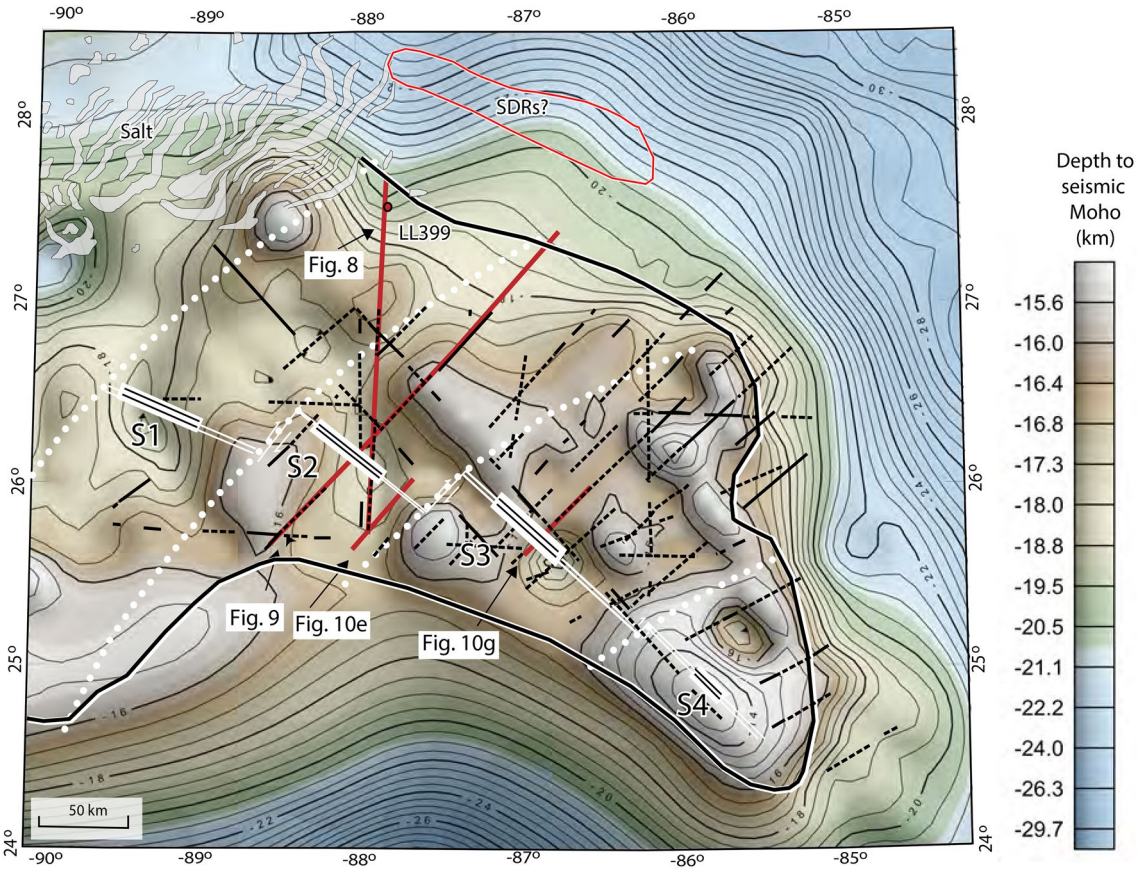

Fig. 14 Map of the seismic Moho interpreted from the industry, 2-D seismic reflection grid shown in Fig. 3a. To complete the map in areas where there is no industry, 2D seismic reflection coverage, the isostatic Moho was used to complete these parts of the Moho map. show the locations of industry seismic lines where the Moho was picked with confidence and dashed lines show locations of seismic lines where the Moho was picked with less confidence. Note the seismic Moho is absent around the mid-ocean ridge (MOR) and in the northwestern EGOM. The map contour interval is 0.5 km

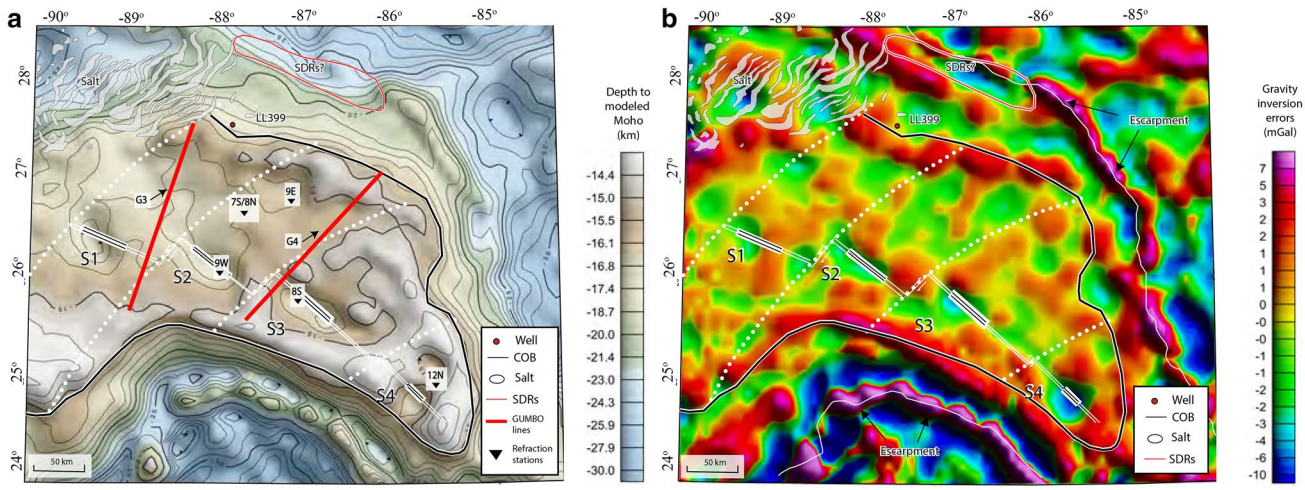

Fig. 15 **a** Moho surface derived from 3-D gravity structural inversion and contoured at an interval of 1 km. Inverted black triangles are refraction station locations used for Moho corrections. The gravity inversion reveals a deep Moho depression parallel to the trend of the mid-ocean ridge segments. **b** Map of the gravity inversion error grid. Most of the inversion error occurs along abrupt, bathymetric scarps formed along the carbonate margins of the conjugate margins in Florida and Yucatan

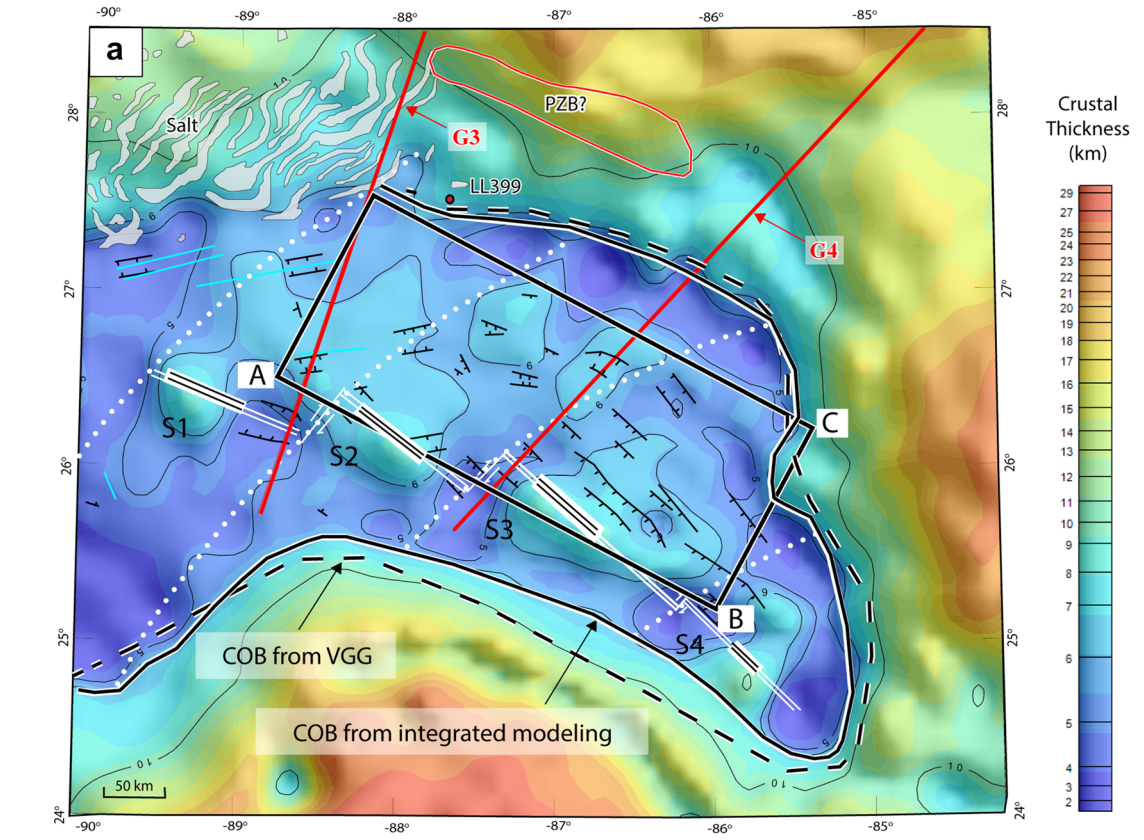
a
Salt
PZB?
G3
G4
LL399
A
B
C
S1
S2
S3
S4
COB from VGG
COB from integrated modeling
50 km
Crustal Thickness (km)
-90°
-89°
-88°
-87°
-86°
-85°
28°
27°
26°
25°
24°

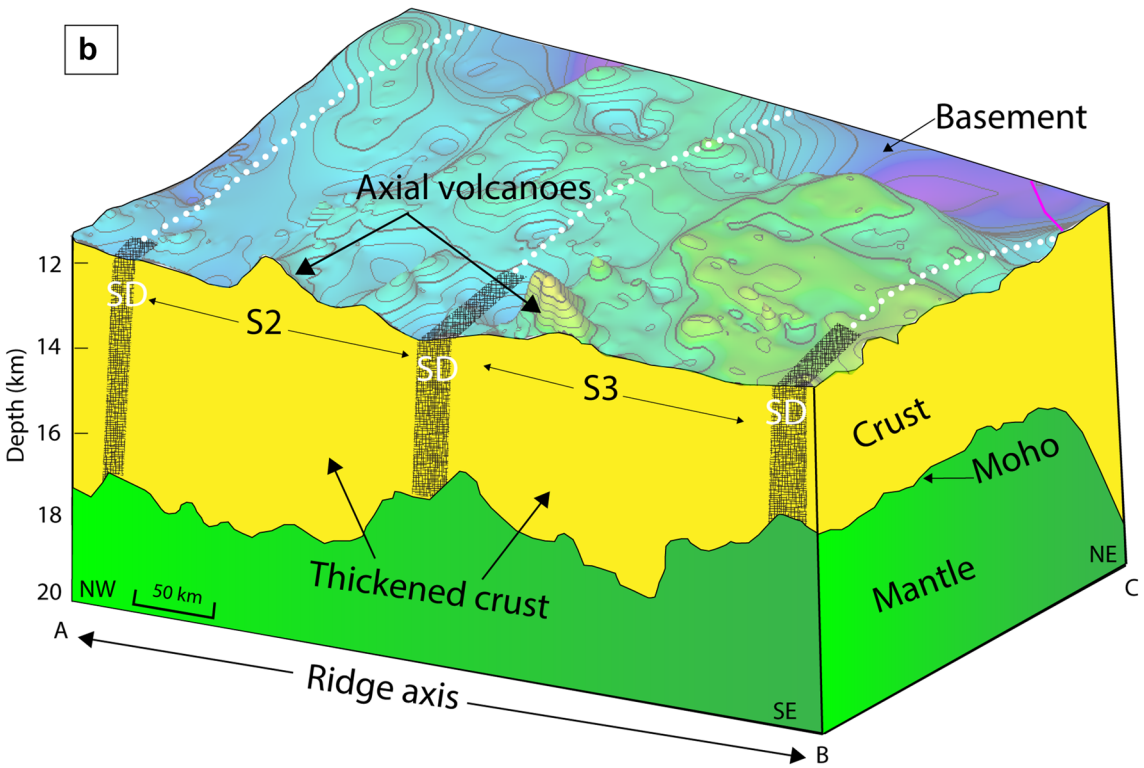
b
Basement
Axial volcanoes
SD
S2
S3
Crust
Moho
Mantle
Thickened crust
NW
NE
SE
50 km
A
B
C
Ridge axis
Depth (km)
12
14
16
18
20

◂**Fig. 16** **a** Crustal thickness map of the eastern Gulf of Mexico (EGOM) based on our basement interpretation and the Moho modeled from the 3D gravity inversion. The red lines are locations of seismic refraction profiles GUMBO 3 (G3) and GUMBO 4 (G4) from Eddy et al. (2018). The orange dashed line is the continent-ocean boundary (COB) from the VGG map (Fig. 1b) and the pink line is the COB from our 3D gravity inversion. The red circle represents the potential Paleozoic basins (PZB?) which was interpreted as seaward dipping reflectors (SDRs) by Imbert (2005a, b). The black rectangle is the location of the area shown schematically in the block diagram in Fig. 16b. **b** The 3-D block diagram shows thicker, oceanic crust (6.5–8.6 km) beneath the spreading centers with off-axis volcanoes located northwest of the spreading center. Second-order discontinuities (SD) separate the two ridge segments and exhibit thinner crust typical for areas of secondary discontinuities (White et al. 1992)

Due to the short time of seafloor spreading before ridge jump, the interpreted earlier ridge is not well expressed on any of our data including the 2D seismic reflection, gravity, and magnetic data. We can only infer the location of earlier ridge from the structure and isopach maps of the Haynesville Formation (Figs. 12a, 13a). The pole of rotation in the earlier phase of seafloor spreading is close to the pole of rotation proposed by Hall and Najmuddin (1994) (Fig. 18c). The later final pole of seafloor spreading is around the pole of rotation in the northwest Cuba which formed the ridge-fracture zone in the middle of oceanic crust observed in the VGG data (Nguyen and Mann 2016) and hotspot tracks on the oceanic crust of central GOM (Bird et al. 2015) (Fig. 18d).

Thickness variations of the EGOM oceanic crust

White et al. (1992) found that the global average thickness of oceanic crystalline crust is 7.1 ± 0.8 km, while Reid and Jackson (1981) reported that the thickness of oceanic crust ranges from 5 to 6.6 km for crust produced along active, slow spreading centers. Van Avendonk et al. (2017) calculated that the average crystalline thickness of Jurassic oceanic crust in the Indian and Pacific is around 7.1 km—or 1.2 km thicker than present-day, oceanic crust. Van Avendonk et al. (2017) attribute these variations to decreasing mantle temperatures following the breakup of Pangaea. The average thickness of the oceanic crust derived from the basement and modeled Moho (Fig. 16) of the EGOM in this study is 6.1 km, which is a typical thickness observed along other, Jurassic slow-spreading centers (Reid and Jackson 1981; Van Avendonk et al. 2017).

Our COB mapping in the thickness map using 6.1 km (Fig. 16) is consistent with the abrupt changes of the Bouguer gravity anomaly and reduced-to-pole magnetic anomaly (Figs. 4a, 5b). In the Bouguer gravity anomaly, the mapped COB lies on the gentle gravity fall from 145 mGal to 80 mGal in the Florida margin (Fig. 4a). In the reduced-to-pole magnetic anomaly, the mapped COB is close to the NW-SE trending magnetic high around 25 nT.

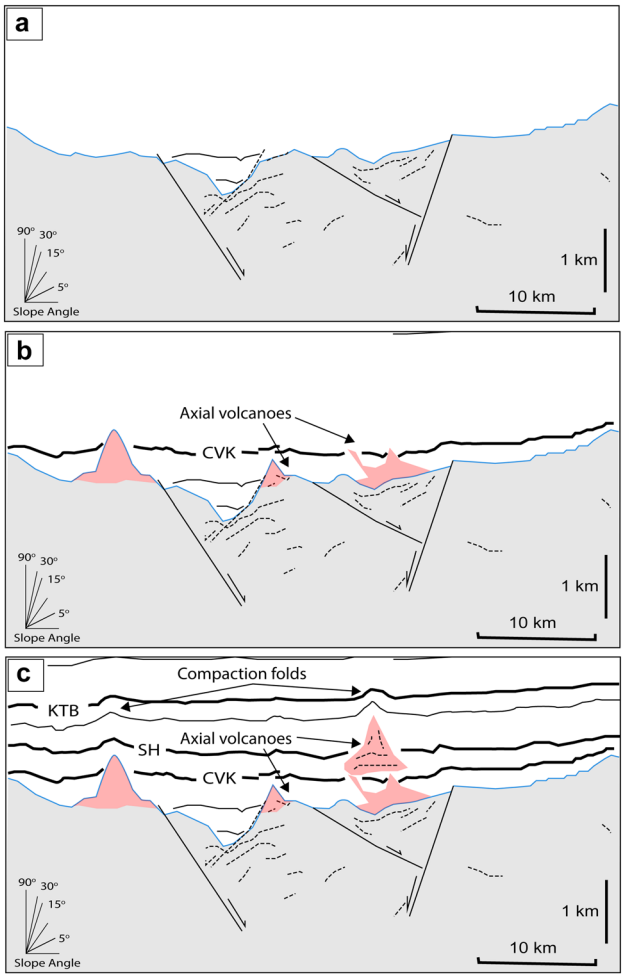

Fig. 17 The evolution of the axial features represented by cross section across ridge segment 2 in Fig. 10g, h. **a** Axial valley formed during slow seafloor spreading. **b** These axial volcanoes formed when spreading ceased - or shortly after. **c** Cretaceous sediments were deposited on the axial volcanoes and became folded over their crests as a result of compaction

In addition, pre-drift salt diapirs are found exactly along the COB identified in the northeastern GOM (Fig. 8). Along interpreted COB, 5–25 km offsets are observed in the residual gravity data and correlate with fracture zone terminations at the continental crust boundary.

In addition to its greater width, the northwestern flank of the ocean floor in the EGOM is slightly thicker (average 6.4 km) than the southeastern flank (average 5.5 km). Each of the four ridge segments is separated by relatively thin crust (5 km) that we infer formed as secondary discontinuities. However, the oceanic crust is thickest in the center of each of the four, spreading ridge segments. This areas of thickened crust (6.4–8.6 km) underlies the centers of the four ridge segments and produces negative residual Bouguer gravity anomalies (Fig. 3b). We then used the

Table 1 Summary of asymmetrical areas of oceanic crust, and excess accretion rate compiled from Müller et al. (2008)

MOR location	Excess plate	Crustal accretion value (%)	Excess accretion rate (%)	Asymmetric spreading age	Related hot spot	Hot spot age
Central North Atlantic Ocean	Newfoundland	53	3	Last 130 Ma	NA	NA
Central North Atlantic Ocean	U.S East Coast	51	1	Last 130 Ma	NA	NA
Gulf of Mexico	Gulf of Mexico	55–60	5–10	158–138 Ma	NA	NA
Equatorial Atlantic Ocean	Demerara Abyssal Plain	55–65	5–15	Last 80 Ma	NA	NA
Southern South Atlantic Ocean	Argentine basin	53–54	3–4	Last 30 Ma	Tristan Da Cunha hot spot	125 Ma
Central Indian Ocean	Bay of Bengal	55–65	5–15	100–80 Ma	NA	NA
West Pacific Ocean	Southwest of the Philippine Sea	60–70	10–20	Last 70 Ma	NA	NA
Australian Antarctic Discordant Zone	Australian plate	52–70	2–20	60–30 Ma	Balleny hot spot	36 Ma
East Pacific Rise	Nazca plate	70	20	Last 20 Ma	Pacific hot spot	NA

The GOM has a relatively high, excess accretion rate of about 5–10%. The age of hot spot is from Steinberger (2000)

6.1 km-thickness contour of the crystalline crust as a constraint for mapping the continent-ocean boundary in the EGOM (Fig. 15a).

Our integrated 3-D crustal model is based on the integration of the 2D seismic reflection grid and the gravity data, and is summarized as a schematic block diagram where crustal sections are drawn both parallel and perpendicular to the extinct ridge of the EGOM (Fig. 16b). Our crustal model is consistent with previous GUMBO seismic refraction results of Christeson et al. (2014) and Eddy et al. (2014, 2018). These groups have all reported that the thickness of oceanic crystalline crust changes from 8 km in northwestern EGOM to 5.6–5.7 km in the central EGOM and suggested that crustal thickening accompanied seafloor spreading in the northwestern GOM (Eddy et al. 2014). The excess magma supply in the northwest EGOM is also supported by high-velocity thick oceanic crust on GUMBO Line 3 (Eddy et al. 2014).

Conclusions

In this study, we generated regional maps of the top and base of interpreted oceanic crust (i.e., top basement and Moho). The seismic grid used was an industry, 2-D, deep-penetration seismic reflection data that covers an area of 120,000 km^2 area in the eastern Gulf of Mexico (Fig. 6a). We combined the seismic reflection mapping results of oceanic basement with mapping results from potential fields and refraction data to describe an interpreted extinct Jurassic oceanic spreading system, now buried beneath 5.5–7-km of earliest Cretaceous to Recent sediments. The main conclusions of this study include the following:

(1) The morphology of 30-60-km-long, northwest-trending, late Jurassic-to-earliest Cretaceous ridge segment characterized by ridge-axis volcanoes located near the centers of inwardly-dipping, normal-fault-bounded, axial valleys. Ridge-axis segments are truncated by northeast-trending, second-order discontinuities with ridge offsets of 5–30 m which contrast with first-order discontinuities transform faults (Fig. 7).

(2) Our integration of residual gravity anomalies with detailed basement mapping from 2D seismic reflection data shows that major basement faults strike northwest and are subparallel to spreading ridge segments S1 to S4. Several northeast-striking, normal faults are possible related to fracture zones (Fig. 7). Both northwest and northeast trends of faults in the oceanic crust indicate a continuous and progressive northwest opening of EGOM and counterclockwise rotation of the Yucatan continental block as proposed by previous workers (Marton and Buffler 1994; Pindell and Kennan 2009; Hudec et al. 2013; Eddy et al. 2014; Nguyen and Mann 2016).

(3) Based on sedimentary layering inferred beneath prominent axial volcanoes erupted at the spreading ridge (Figs. 3, 10), we propose that these large volcanoes formed near the end, or soon after, the cessation of late Jurassic-to-earliest Cretaceous seafloor spreading and reflect an excess magma supply produced by a fertile mantle (Fig. 10).

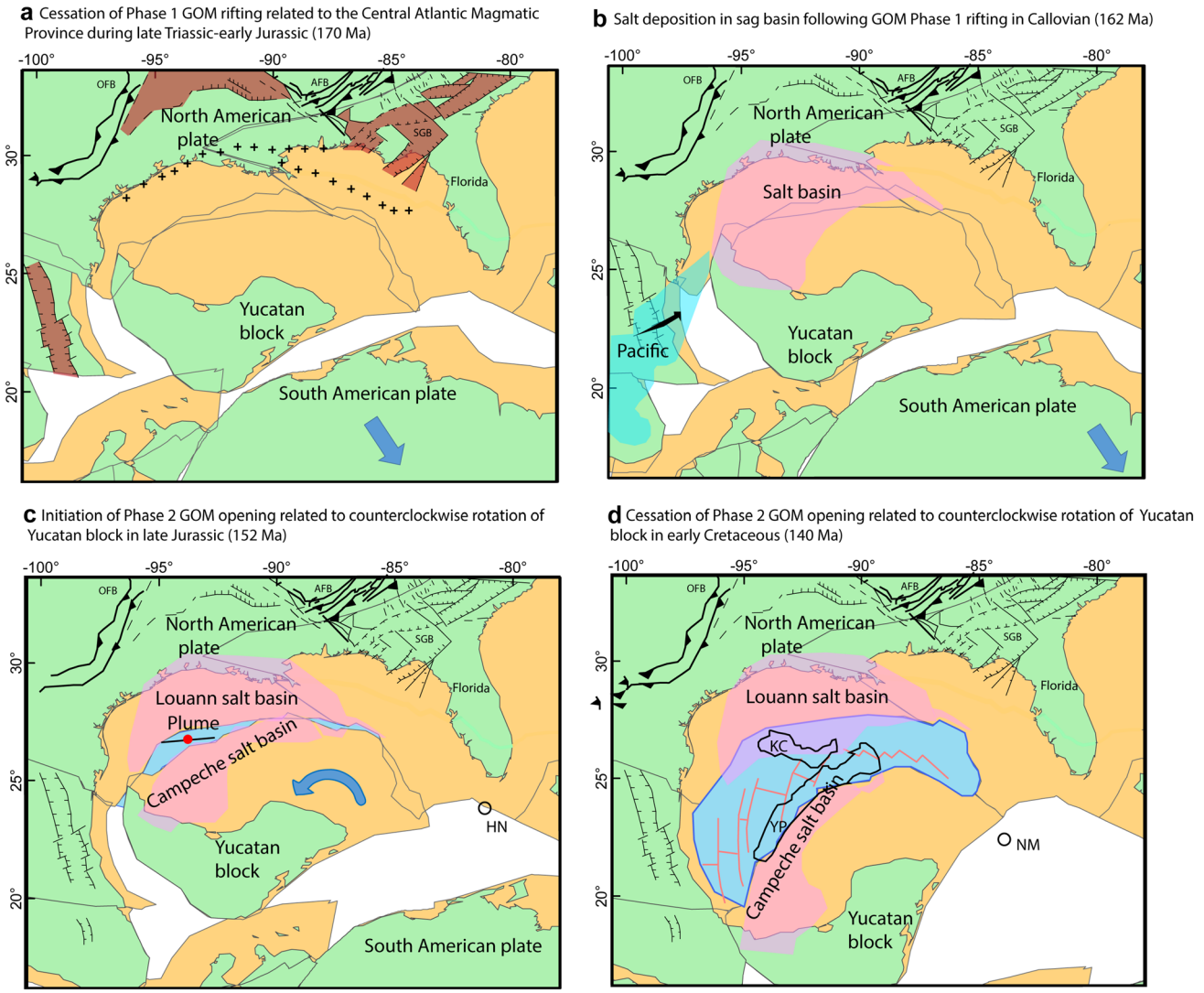

Fig. 18 Opening of the GOM related to the presence of a mantle plume from Triassic to the earliest Cretaceous. Ouachita-Appalachian fold-thrust belt (OFB and AFB) and associated foreland basins are older features formed during late Paleozoic collision (Nance et al. 2012). SGB-South Georgia Basin (McBride and Nelson 1988). **a** Cessation of Phase 1 GOM rifting coincided with the eruption of the Central Atlantic Magmatic Province (CAMP) during late Triassic-early Jurassic (170 Ma). The presence of CAMP is indicated by the radial dike swarms in the southeastern USA (Byerly 1991). **b** Salt deposition in a large sag basin followed GOM Phase 1 rifting during Callovian (162 Ma). The salt distribution is from Lin (2018). **c** Initiation of Phase 2 GOM opening was related to counterclockwise rotation of Yucatan in late Jurassic (152 Ma). The pole of rotation (HN) is from Hall and Najmuddin (1994). After the mantle plume formed in the central GOM, the spreading ridge jumped towards the southwest. The location of the mantle plume is from Bird et al. (2005). **d** Cessation of Phase 2 GOM opening is related to counterclockwise rotation of Yucatan block in the earliest Cretaceous. The later pole of rotation (NM) for Phase 2 opening is from Nguyen and Mann (2016). The hotspot tracks called Keathley Canyon (KC) and Yucatan parallel (YP) formed during Phase 2 seafloor spreading (Bird et al. 2005)

(4) Asymmetry of the oceanic crust in the EGOM study area with the wider (55–60%), oceanic limb located to the northwest of the spreading center can be explained by the presence of an earlier—but previously unrecognized—late Jurassic-to-earliest Cretaceous, spreading ridge—that was abandoned when the spreading ridge jumped to the southwest.

(5) Using high-resolution and deep-penetrating seismic reflection data, we identified a series of Lower Crustal Dipping Reflectors (LCDR) and a velocity sublayer within the oceanic crust previously defined from refraction data. The distribution of basement faults and LCDR's lead us to propose that this sublayer is a brittle-ductile boundary within the oceanic crust (Fig. 9).

(6) Integrated 3-D structural gravity inversion, constrained by seismic refraction data from published sources and the results of our reflection seismic interpretation of the Spectrum Geo data show a thicker crust (6.4 km) in the northwestern EGOM as supported by the presence of thicker (> 8 km) oceanic crust on GUMBO 3 refraction profile (Eddy et al. 2014). This thicker crust in the northwestern part of the EGOM indicates increased magma supply during seafloor spreading (Fig. 16).

(7) Modeled thicknesses of the crystalline crust in the extinct spreading ridge segments (6.4–8.6-km) are greater in the central parts of the 30–60-km-long ridge segments, possibly indicating the presence of a low-density gabbro root (Fig. 16).

Acknowledgements We thank Mike Saunders at Spectrum Geo for providing the extensive, 2D grid of seismic reflection data that was critical for this study and for providing us permission to publish these results. We thank Gyorgy Marton and Julia Wellner for valuable discussions and Geosoft for providing the University of Houston with the Oasis Montaj potential field interpretation software. Finally, we thank the industry sponsors of the Conjugate Basins, Tectonics, and Hydrocarbons Consortium at the University of Houston for their continued financial support. We thank Ted Godo (Murphy Oil) and Van Mount (Anadarko) for their constructive reviews for this journal.

References

Ángeles-Aquino FJ, Cantú-Chapa A (2001) Chap. 14: Subsurface Upper Jurassic stratigraphy in the Campeche Shelf, Gulf of Mexico. In: Bartolini C, Buffler RT, Cantú-Chapa A (eds), The western Gulf of Mexico Basin. Tectonics, sedimentary basins, and petroleum systems. AAPG Memoir 75, Tulsa, 343–352

Barckhausen U, Engels M, Franke D, Ladage S, Pubellier M (2014) Evolution of the South China Sea: revised ages for breakup and seafloor spreading. Mar Pet Geol 58:599–611

Bécel A, Shillington DJ, Nedimović MR, Webb SC, Kuehn H (2015) Origin of dipping structures in fast-spreading oceanic lower crust offshore Alaska imaged by multichannel seismic data. Earth Planet Sci Lett 424:26–37

Besse J, Courtillot V (2002) Apparent and true polar wander and the geometry of the geomagnetic field over the last 200 Myr. J Geophys Res 107(B11):2300

Bird D, Burke K, Hall S, Casey J (2005) Gulf of Mexico tectonic history: hotspot tracks, crustal boundaries, and early salt distribution. AAPG Bull 89(3):311–328

Blakely R (1995) Potential theory in gravity and magnetic applications. Cambridge University Press, Cambridge

Byerly GR (1991) Igneous activity, the Gulf of Mexico Basin. In: Salvador A (ed), The Geology of North America J. GSA, Boulder, 91–108

Christeson G, Van Avendonk H, Norton I, Snedden J, Eddy D, Karner G, Johnson C (2014) Deep crustal structure in the eastern Gulf of Mexico. J Geophys Res 119(9):6782–6801

Cordell L (1973) Gravity analysis using an exponential density-depth function: San Jacinto graben, California. Geophysics 38(4):684–690

Cregg AK, Ahr WM (1984) Paleoenvironment of an upper Cotton Valley (Knowles Limestone) patch reef, Milam County, Texas. In: Ventress WPS, Bebout DG, Perkins BF, and Moore CH (eds) The Jurassic of the Gulf rim: Gulf Coast Section, SEPM, proceedings of the third annual research conference, pp 41–56

Deighton IC, Winter F, Chisari D (2017) Recent high-resolution seismic, magnetic and gravity data throws new light on the early development of the Gulf of Mexico. In AAPG Annual Meeting Abstracts, Houston

Dobson LM, Buffler RT (1997) Seismic stratigraphy and geological history of Jurassic rocks, northeastern Gulf of Mexico. AAPG Bull 81(1):100–120

Ebeniro JO, O'Brien WP, Shaub FJ (1986) Crustal structure of the South Florida platform, eastern Gulf of Mexico: an ocean-bottom seismograph refraction study. Mar Geophys Res 8(4):363–382

Eddy D, Van Avendonk H, Christeson G, Norton I, Karner G, Johnson C, Snedden J (2014) Deep crustal structure of the northeastern Gulf of Mexico: implications for rift evolution and seafloor spreading. J Geophys Res 119(9):6802–6822

Eddy D, Van Avendonk H, Christeson G, Norton I (2018) Structure and origin of the rifted margin of the northern Gulf of Mexico. Geosphere 14(4):1–14

Escalona A, Yang W (2013) Subsidence controls on foreland basin development of northwestern offshore Cuba, southeastern Gulf of Mexico subsidence controls, northwestern Offshore Cuba. AAPG Bull 97(1):1–25

Finn C, Pilkington M, Cuevas A, Hernandez I, Urrutia J (2001) New digital magnetic anomaly database for North America. Lead Edge 20(8):870–872

Fox PJ, Gallo DG (1984) A tectonic model for ridge-transform-ridge plate boundaries: Implications for the structure of oceanic lithosphere. Tectonophysics 104(3–4):205–242

Galloway WE (2008) Depositional evolution of the Gulf of Mexico sedimentary basin. In: Miall AD (ed), Sedimentary basins of the world 5, pp 505–549

Galloway W, Ganey-Curry P, Li X, Buffler RT (2000) Cenozoic depositional history of the Gulf of Mexico basin. AAPG Bull 84(11):1743–1774

Goldhammer RK, Johnson CA (2001) Middle Jurassic-Upper Cretaceous paleogeographic evolution and sequence-stratigraphic framework of the northwest Gulf of Mexico rim. In: Bartolini C, Buffler RT, Cantú-Chapa A (eds), The western Gulf of Mexico Basin: tectonics, sedimentary basins, and petroleum systems. AAPG Memoir 75, pp 45–81

Haase K, Regelous M, Duncan R, Brandl P, Stroncik N, Grevemeyer I (2011) Insights into mantle composition and mantle melting beneath midocean ridges from post-spreading volcanism on the fossil Galapagos Rise. Geochem Geophys Geosyst 12(5):1–21

Hall S, Najmuddin IJ (1994) Constraints on the tectonic development of the eastern Gulf of Mexico provided by magnetic anomaly data. J Geophys Res 99(B4):7161–7175

Hall S, Casey J, Elthon D (1986) A possible explanation of gravity anomalies over mid-ocean ridges. J Geophys Res 91(B3):3724–3738

Hey RN (1977) A new class of pseudofaults and their bearing on plate tectonics: a propagating rift model. Earth Planet Sci Letters 37:321–325

Hudec M, Norton I, Jackson M, Peel F (2013) Jurassic evolution of the Gulf of Mexico salt basin. AAPG Bull 97(10):1683–1710

Ibrahim A, Carye J, Latham G, Buffler R (1981) Crustal structure in Gulf of Mexico from OBS refraction and multichannel reflection data. AAPG Bull 65(7):1207–1229

Imbert P (2005a) The Mesozoic opening of the Gulf of Mexico: part 1, Evidence for oceanic accretion during and after salt deposition. In: Post PJ et al. (ed), Transactions of the 25th annual GCSSEPM

research conference: petroleum systems of divergent continental margins, SEMP, Tulsa, pp 1119–1150
Imbert P, Philippe Y (2005b) The Mesozoic opening of the Gulf of Mexico: part 2, Integrating seismic and magnetic data into a general opening model. In: Post PJ et al. (ed) Transactions of the 25th annual GCSSEPM research conference: petroleum systems of divergent continental margins, SEPM, Tulsa, pp 1151–1189
Jakobsson M, Mayer LA, Coakley B, Dowdeswell JA, Forbes S, Fridman B, Hodnesdal H, Noormets R, Pedersen R, Rebesco M, Schenke H-W, Zarayskaya Y, Accettella AD, Armstrong A, Anderson RM, Bienhoff P, Camerlenghi A, Church I, Edwards M, Gardner JV, Hall JK, Hell B, Hestvik OB, Kristoffersen Y, Marcussen C, Mohammad R, Mosher D, Nghiem SV, Pedrosa MT, Travaglini PG, Weatherall P (2012) The international bathymetric chart of the Arctic Ocean (IBCAO) version 3.0. Geophys Res Lett 39(12):1–6
Jonas J, Hall S, Casey J (1991) Gravity anomalies over extinct spreading centers: a test of gravity models of active centers. J Geophys Res 96(B7):11759–11777
Kegel J, Chaikin D, Torry B (2016) New insights from 3D data over an extinct spreading ridge and its implications to deepwater offshore exploration. GCAGS Trans 66:307–312
Kleinrock Martin C, Tucholke BE, Lin J, Tivey MA (1997) Fast rift propagation at a slow-spreading ridge. Geology 25(7), 639–642
Lin P (2018) Crustal structure and tectonostratigraphic evolution of the eastern Gulf of Mexico basin. Ph.D. dissertation, University of Houston, pp 141
Liu B, Li SZ, Jiang SH, Suo YH, Guo LL, Wang YM, Zhang HX (2017) Origin and model of transform faults in the Okinawa Trough. Mar Geophys Res 38(1–2):137–147
Macdonald K, Scheirer D, Carbotte S, Fox P (1993) It's only topography: part 2. GSA Today 3(1):29–35
Mammerickx J, Sandwell D (1986) Rifting of old oceanic lithosphere. J Geophys Res: Solid Earth 91(B2):1975–1988
Mammerickx J, Naar DF, Tyce RL (1988) The Mathematician paleoplate. J Geophys Res: Solid Earth 93(B4):3025–3040
Marton G (1995) Jurassic evolution of the southeastern Gulf of Mexico. Ph.D. dissertation, University of Texas at Austin, Austin, pp 276
Marton G, Buffler R (1994) Comment on Jurassic reconstruction of the Gulf of Mexico Basin. Int Geol Rev 36(6):545–586
Marton G, Buffler R (1999) Jurassic-early Cretaceous tectono-paleogeographic evolution of the southeastern Gulf of Mexico basin. Sedimentary Basins of the World 4, Elsevier, pp 63–91
May PR (1971) Pattern of Triassic-Jurassic diabase dikes around the North Atlantic in the context of predrift position of the continents. Geol Soc Am Bull (82): 1285–1292
McBride JH, Nelson KD (1988) Integration of COCORP deep reflection and magnetic anomaly analysis in the southeastern United States: implications for origin of the Brunswick and East Coast magnetic anomalies. Geol Soc Am Bull 100(3):436–445
Morris E, Detrick R, Minshull T, Mutter J, White R, Su W, Buhl P (1992) Seismic structure of oceanic crust in the western North Atlantic. J Geophys Res 98(B8):13879–13903
Müller RD, Sdrolias M, Gaina C and, and Roest WR (2008) Age, spreading rates, and spreading asymmetry of the world's ocean crust. Geochem Geophys Geosyst 9(4)
Mutter J, Karson J (1992) Structural processes at slow-spreading ridges. Science 257(5070):627–634
Nance RD, Gutiérrez-Alonso G, Keppie JD, Linnemann U, Murphy JB, Quesada C, Strachan RA, Woodcock NH (2012) A brief history of the Rheic Ocean. Geosci Front 3(2):125–135
Nguyen L, Mann P (2016) Gravity and magnetic constraints on the Jurassic opening of the oceanic Gulf of Mexico and the location and tectonic history of the Western Main transform fault along the eastern continental margin of Mexico. Interpretation 4(1):SC23–SC33
Osler J, Louden K (1995) Extinct spreading center in the Labrador Sea: Crustal structure from a two-dimensional seismic refraction velocity model. J Geophys Res 100(B2):2261–2278
Parker R (1973) The rapid calculation of potential anomalies. Geophys J Int 31(4):447–455
Pindell J, Kennan L (2009) Tectonic evolution of the Gulf of Mexico, Caribbean and northern South America in the mantle reference frame: an update. In James KH, Lorente MA, Pindell JL (eds), The origin and evolution of the caribbean plate. Geo Soc London Spec Publ, Geological Society, London 328(1): pp 1–55
Pindell J, Miranda CE, Cerón A, Hernandez L (2016) Aeromagnetic map constrains Jurassic–Early Cretaceous synrift, break up, and rotational seafloor spreading history in the Gulf of Mexico, Mesozoic of the Gulf Rim and Beyond: New Progress in Science and Exploration of the Gulf of Mexico Basin. In: Lowery CM, Snedden JW, Rosen NC (eds), 35th Annual Gulf Coast section SEPM foundation Perkins-Rosen research conference, GCSSEPM Foundation, Houston, TX, USA: 123–153
Ranero C, Banda E, Buhl P (1997a) The crustal structure of the Canary Basin: Accretion processes at slow spreading centers. J Geophys Res 102(B5):10185–10201
Ranero CR, Reston TJ, Belykh I, Gribidenko H (1997b) Reflective crust formed at a fast-spreading center in the Pacific. Geology 25(6):499–502
Reid I, Jackson H (1981) Oceanic spreading rate and crustal thickness. Mar Geophys Res 5(2):165–172
Row L, Dunbar P, Hastings D (1995) TerrainBase: Worldwide digital terrain data. National Geophysical Data Center, available online at http://www.ngdc.noaa.gov
Salvador A (1991) Triassic-Jurassic, the Gulf of Mexico Basin. In: Salvador A (ed) The Geology of North America J. Geological Society of America, Boulder, Colorado, pp 131–18
Sandwell DT, Smith WHF (2009) Global marine gravity from retracked Geosat and ERS-1 altimetry: Ridge segmentation versus spreading rate. J Geophys Res 114 B01411
Sandwell D, Müller R, Smith W, Garcia E, Francis R (2014) New global marine gravity model from CryoSat-2 and Jason-1 reveals buried tectonic structure. Science 346(6205):65–67
Sawyer DS, Buffler RT, Pilger RH Jr (1991) The crust under the Gulf of Mexico Basin. In: Salvador A (ed), Gulf of Mexico Basin. Geol Soc of America, The Geology of North America, Boulder, pp 53–72
Schultz R, Okubo C, Wilkins S (2006) Displacement-length scaling relations for faults on the terrestrial planets. J Struct Geol 28(12):2182–2193
Snedden J, Eddy D, Christeson G, Van Avendonk H, Olson H, Ganey-Curry P, Norton I (2013) A new temporal model for eastern Gulf of Mexico Mesozoic deposition. GCAGS Trans 63:609–612
Snedden J, Norton I, Christeson G, Sanford J (2014) Interaction of deepwater deposition and a mid-ocean spreading center, eastern Gulf of Mexico Basin, USA. GCAGS Trans 64:371–383
Steinberger B (2000) Plumes in a convecting mantle: models and observations for individual hotspots. J Geophys Res 105(B5):11127–11152
Stephens B (2001) Basement controls on hydrocarbon systems, depositional pathways, and exploration plays beyond the Sigsbee Escarpment in the central Gulf of Mexico. In: Proceedings 21st annual GCSSEPM foundation Bob F. Perkins research conference, petroleum systems of deep-water basins: Global and Gulf of Mexico Experience, pp 129–157
Taylor B, Goodliffe AM, Martinez F (1999) How continents break up: Insights from Papua New Guinea. J Geophys Res 104(B4):7497–7512
Van Avendonk HJ, Davis JK, Harding JL, Lawver LA (2017) Decrease in oceanic crustal thickness since the breakup of Pangaea. Nat Geosci 10(1):58–61

White RS (2012) Wide-angle refraction and reflection. Regional Geology & Tectonics Principles of Geologic Analysis, 310–328
White R, Detrick R, Mutter J, Buhl P, Minshull T, Morris E (1990) New seismic images of oceanic crustal structure. Geology 18(5):462–465
White R, McKenzie D, O'Nions R (1992) Oceanic crustal thickness from seismic measurements and rare earth element inversions. J Geophys Res 97(B13):19683–19715
Whittaker J, Goncharov A, Williams S, Müller R, Leitchenkov G (2013) Global sediment thickness dataset updated for the Australian-Antarctic Southern Ocean. Geochem Geophys Geosyst 14(8):3297–3305
Zhao M, Sibuet J, He E, Tan P, Wang J, Qiu X (2016) The formation of post-spreading volcanic ridges in the South China Sea. In: EGU General Assembly Conference Abstracts 18:3239